




# Genetic and pharmacological inhibition of the nuclear receptor ROR $\alpha$ regulates T<sub>H</sub>17 driven inflammatory disorders

Ran Wang<sup>1,5,7</sup>, Sean Campbell<sup>1,7</sup>, Mohammed Amir<sup>1,6,7</sup>, Sarah A. Mosure<sup>1,2,3</sup>, Molly A. Bassette<sup>1</sup>, Amber Eliason<sup>1</sup>, Mark S. Sundrud<sup>1</sup>, Theodore M. Kamenecka<sup>4</sup> & Laura A. Solt<sup>1,4</sup>✉

Full development of IL-17 producing CD4<sup>+</sup> T helper cells (T<sub>H</sub>17 cells) requires the transcriptional activity of both orphan nuclear receptors ROR $\alpha$  and ROR $\gamma$ t. However, ROR $\alpha$  is considered functionally redundant to ROR $\gamma$ t; therefore, the function and therapeutic value of ROR $\alpha$  in T<sub>H</sub>17 cells is unclear. Here, using mouse models of autoimmune and chronic inflammation, we show that expression of ROR $\alpha$  is required for T<sub>H</sub>17 cell pathogenicity. T-cell-specific deletion of ROR $\alpha$  reduces the development of experimental autoimmune encephalomyelitis (EAE) and colitis. Reduced inflammation is associated with decreased T<sub>H</sub>17 cell development, lower expression of tissue-homing chemokine receptors and integrins, and increased frequencies of Foxp3<sup>+</sup> T regulatory cells. Importantly, inhibition of ROR $\alpha$  with a selective small molecule antagonist mostly phenocopies our genetic data, showing potent suppression of the *in vivo* development of both chronic/progressive and relapsing/remitting EAE, but with no effect on overall thymic cellularity. Furthermore, use of the ROR $\alpha$  antagonist effectively inhibits human T<sub>H</sub>17 cell differentiation and memory cytokine secretion. Together, these data suggest that ROR $\alpha$  functions independent of ROR $\gamma$ t in programming T<sub>H</sub>17 pathogenicity and identifies ROR $\alpha$  as a safer and more selective therapeutic target for the treatment of T<sub>H</sub>17-mediated autoimmunity.

<sup>1</sup>Department of Immunology and Microbiology, The Scripps Research Institute, Jupiter, FL 33458, USA. <sup>2</sup>Department of Integrative Structural and Computational Biology, The Scripps Research Institute, Jupiter, FL 33458, USA. <sup>3</sup>Skaggs Graduate School of Chemical and Biological Sciences, The Scripps Research Institute, Jupiter, FL 33458, USA. <sup>4</sup>Department of Molecular Medicine, The Scripps Research Institute, Jupiter, FL 33458, USA. <sup>5</sup>Present address: Mater Research Institute, The University of Queensland, Woolloongabba, QLD 4102, Australia. <sup>6</sup>Present address: Gale and Ira Drukier Institute for Children's Health, Department of Pediatrics, Weill Cornell Medicine, New York, NY 10021, USA. <sup>7</sup>These authors contributed equally: Ran Wang, Sean Campbell, Mohammed Amir. ✉email: [lsolt@scripps.edu](mailto:lsolt@scripps.edu)

Helper 17 (T<sub>H</sub>17) cells are an important lineage of CD4<sup>+</sup> T effector (Teff) cells that survey mucosal barriers, secrete IL-17-family cytokines, and guard against extracellular bacteria and fungi at mucosal surfaces. Patients with defects in the T<sub>H</sub>17 pathway, including autosomal dominant Hyper-IgE syndrome (AD-HIES), suffer from recurrent infections to mucocutaneous fungal and bacterial infections, such as *Candida albicans* and *Staphylococcus aureus*<sup>1–3</sup>. In contrast, over-exuberant T<sub>H</sub>17 responses have been implicated in many human autoimmune diseases, including multiple sclerosis, rheumatoid arthritis, and inflammatory bowel disease (IBD)<sup>4</sup>. Genome-wide association studies indicate SNPs in multiple genes associated with the T<sub>H</sub>17 axis as susceptibility factors in autoimmunity<sup>5,6</sup>. As a consequence, a large effort has been put forth to target this pathway for the treatment of T<sub>H</sub>17-mediated diseases, and in particular to identify pharmacologically accessible mechanisms that block pathogenic, but not protective, T<sub>H</sub>17 cell functions.

The nuclear receptor (NR) retinoic acid receptor-related orphan receptor gamma t (RORγt; NR1F3) is considered the lineage defining transcription factor of T<sub>H</sub>17 cells<sup>7</sup>. Since its discovery over a decade ago, a significant amount of work has been invested into understanding RORγt's function in T<sub>H</sub>17 cells, and to translate this understanding into new treatments for autoimmune and inflammatory syndromes. While RORγt is critical for T<sub>H</sub>17 cell development, IL-17A is not completely abolished in RORγt-deficient mice; its close family member, RORα (NR1F1), is also required for full T<sub>H</sub>17 cell development<sup>8</sup>. Thus, deletion of both receptors completely abolishes T<sub>H</sub>17 cell development<sup>8</sup>. Despite this, RORα is considered redundant to RORγt and as such the functions of RORα in protective and pathogenic T<sub>H</sub>17 cell responses have not been systematically explored.

Here we show that RORα is a critical factor required for the development of autoimmunity and chronic inflammatory responses using mouse models of multiple sclerosis and colitis. Importantly, as a member of the nuclear receptor superfamily, RORα is a ligand-regulated transcription factor and targeting of this receptor in vivo not only inhibits the development of autoimmunity, it effectively suppresses active inflammation. These effects extend to human T<sub>H</sub>17 cells, both during differentiation and in the regulation of pro-inflammatory cytokine expression in lineage-committed T<sub>H</sub>17 cell memory subsets. Unlike pharmacologic inhibition of RORγt, we show that RORα inhibition suppresses pro-inflammatory T<sub>H</sub>17-responses while inducing immunoregulatory function, while leaving thymic T cell development intact. Collectively, these data suggest that RORα is a non-redundant factor that is required for pathogenic T<sub>H</sub>17 cell function and represents an attractive alternative for treating T<sub>H</sub>17-associated inflammatory diseases in humans.

## Results

### RORα expression is sufficient to drive T<sub>H</sub>17 signature genes.

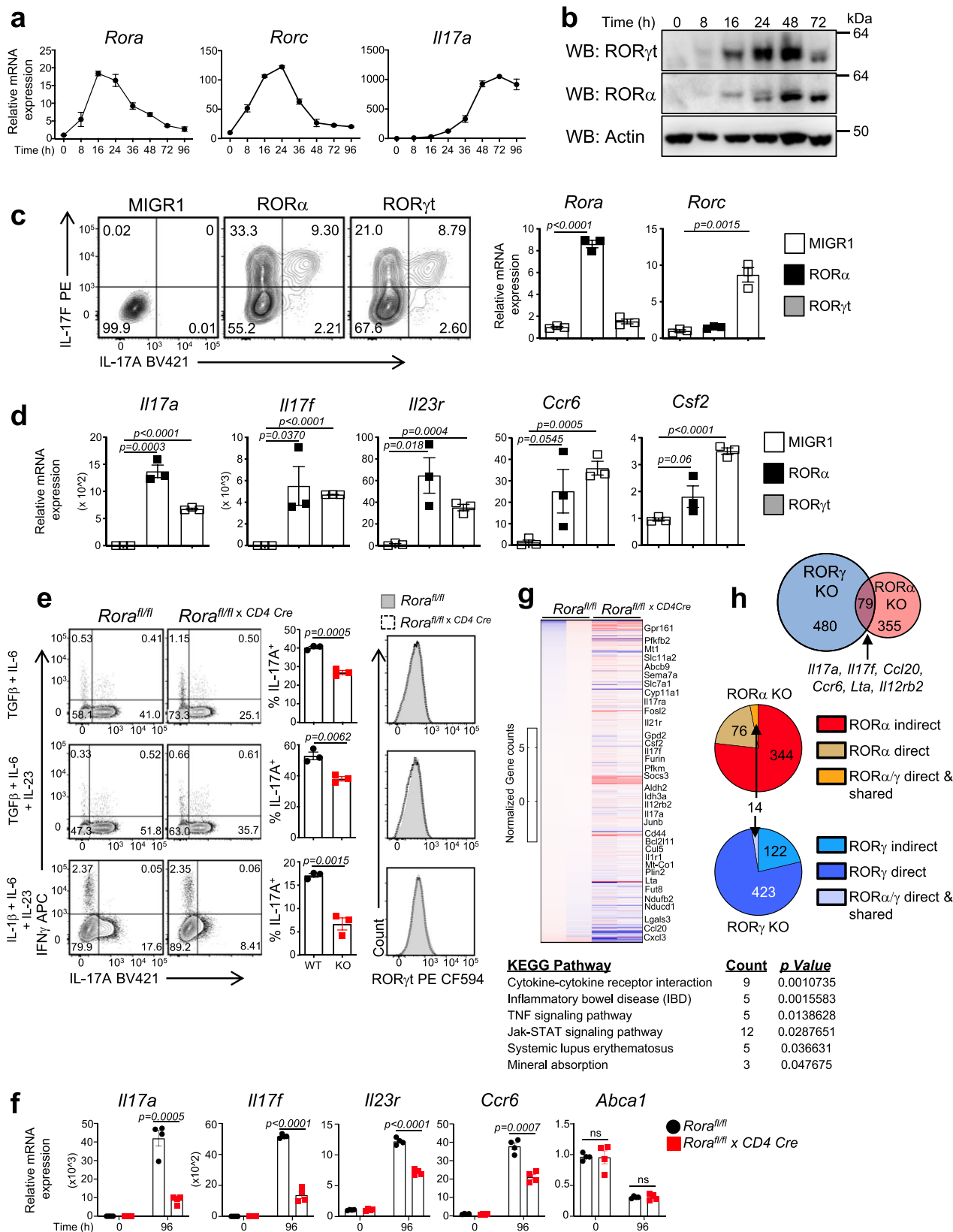
While RORα has been reported to be expressed in T<sub>H</sub>17 cells, we wanted to establish its kinetic expression pattern during T<sub>H</sub>17 cell development<sup>8</sup>. Naïve CD4<sup>+</sup> T cells were differentiated under T<sub>H</sub>17 polarizing conditions (TGFβ + IL-6) to assess the mRNA and protein expression of RORα versus RORγt. Quantitative real-time polymerase chain reaction (qRT-PCR) analysis demonstrated that RORα (*Rora*) was upregulated at similar time points as RORγt (*Rorc*) driving *Il17a* expression<sup>7</sup> (Fig. 1a). This data is consistent with microarray analysis demonstrating that *Rora* is upregulated in both pathogenic and non-pathogenic T<sub>H</sub>17 cells to levels equal to or greater than *Rorc*<sup>9</sup>. Western blot analysis confirmed that RORα was expressed at the protein level (Fig. 1b).

To determine whether RORα alone was sufficient to drive IL-17A and T<sub>H</sub>17-specific gene expression, we retrovirally

overexpressed empty vector (MIGR1), RORα, or RORγt under T<sub>H</sub> neutral conditions (αIL-4 + αIFNγ, no cytokines) in stimulated naïve CD4<sup>+</sup> T cells to assess IL-17A/F expression by flow cytometry. Neutral conditions were used to not confound results since TGFβ and IL-6 upregulate both RORs<sup>8,10,11</sup>. RORα was able to induce IL-17A expression, as was RORγt (Fig. 1c). GFP<sup>+</sup> cells were sorted to perform qRT-PCR to compare RORα vs. RORγt's ability to drive gene expression. RORα induced the expression of *Il17a*, *Il17f*, *Il23r*, *Ccr6*, and *Csf2*, all genes that are considered “core” RORγt target genes<sup>12</sup> (Fig. 1d). These data demonstrate that RORα is capable of driving the T<sub>H</sub>17 cell developmental program.

Previous studies assessing RORα's function in the immune system utilized the *Staggerer* (*Rora*<sup>sg/sg</sup>) mouse, a naturally occurring mutant mouse strain that renders RORα inactive<sup>13</sup>. To more specifically assess the role of RORα in mature CD4<sup>+</sup> T cell responses, we developed RORα “floxed” mice and bred them with *Cd4* Cre mice to delete RORα from T cells (Supplementary Fig. 1A). Differentiation of naïve CD4<sup>+</sup> T cells under non-pathogenic and pathogenic T<sub>H</sub>17 inducing conditions [TGFβ + IL-6 (*top panels*); TGFβ + IL-6 + IL-23 (*middle panels*); IL-6 + IL-1β + IL-23 (*bottom panels*)] from *Rora*<sup>fl/fl</sup> and *Rora*<sup>fl/fl</sup> × *CD4* Cre mice indicated that despite equal amount of RORγt expression between WT and KO conditions, cells lacking RORα were unable to express IL-17A at similar levels as RORα sufficient cells (Fig. 1e). Consistent with previous reports, RORγt-deficient cells had a decreased ability to produce IL-17A<sup>14</sup> indicating that combined expression of both RORs is required for full IL-17A expression (Supplementary Fig. 1B). We observed no difference in the development of naïve CD4<sup>+</sup> T cells into T<sub>H</sub>0, T<sub>H</sub>1, T<sub>H</sub>2, inducible T regulatory (iTregs) or regulatory T (Tr1) cells from *Rora*<sup>fl/fl</sup> and *Rora*<sup>fl/fl</sup> × *CD4* Cre mice (Supplementary Fig. 1C). qRT-PCR analysis of T<sub>H</sub>17 cells cultured under non-pathogenic and pathogenic T<sub>H</sub>17 inducing conditions (see Fig. 1e for conditions) demonstrated that RORα deficiency reduced T<sub>H</sub>17-specific gene expression, including *Il17a*, *Il17f*, *Il23r*, and *Ccr6* whereas no difference was observed in the expression of *Abca1* (Fig. 1f and Supplementary Fig. 2A, B).

To gain a more global understanding of how RORα affects T<sub>H</sub>17 cell development, we performed RNA-sequencing on T<sub>H</sub>17 cells from *Rora*<sup>fl/fl</sup> and *Rora*<sup>fl/fl</sup> × *CD4* Cre mice (Fig. 1g). KEGG pathway analysis indicated RORα was involved in regulation of cytokine–cytokine receptor interactions, inflammatory bowel disease, TNF signaling pathways, and Jak-STAT signaling pathways. We compared our data to RORγt-deficient T<sub>H</sub>17 cells and found that RORα had a smaller gene signature than RORγt<sup>12</sup>, with only 79 genes in common between the two receptors in T<sub>H</sub>17 cells, including “core” RORγt target genes<sup>12</sup> (*Il17a*, *Ccr6*, *Ccl20*, etc.) suggesting RORα and RORγt shared regulation of these genes, which is consistent with the little that is known about RORα's role in T<sub>H</sub>17 cells<sup>8</sup> (Fig. 1h). To begin to address RORα- and RORγt-direct vs. indirect target genes, we compared gene expression in RORα- and RORγt-deficient T<sub>H</sub>17 cells relative to RORα vs. RORγt cistromes from liver and T<sub>H</sub>17 cells, respectively<sup>12,15</sup>. The RORα liver cistrome will still give some indication of RORα direct target genes in tissues. Using this approach, we identified a small number of shared RORα/γt-direct target genes, including *Furin*, *Il17ra*, and *Il1r1*. While our analysis indicated a large number of RORα indirect target genes, including *Il17a*, *Ccl20*, *Socs3*, and *Ccr6*, this may be a consequence of probing the RORα cistrome in a tissue other than T cells. However, a number of interesting direct RORα (only) target genes were uncovered, including those located in the mitochondrial membrane, *Slc11a2*, *Idh3a*, *Gpd2*, and *Ndufb2*, suggesting RORα may play a role in the regulation of mitochondrial metabolism. T<sub>H</sub>17 pathogenicity has been shown to be regulated by high rates



of cellular metabolism and changes in glycolysis, OXPHOS, fatty acid or glutamine metabolism can prevent TH17-mediated autoimmune disease<sup>16–22</sup>. Given most of these genes were downregulated, decreased OXPHOS could be a contributing

factor to the decreased TH17 responses in vitro. Interestingly, *Fosl2*, previously identified as a key TH17 regulator<sup>12</sup>, also appears to be directly regulated by RORα. Given it acts as a repressor, regulation of *Fosl2* expression could also account for the

**Fig. 1 ROR $\alpha$  is expressed and required for full T<sub>H</sub>17 cell differentiation.** **a** Quantitative real-time PCR (qRT-PCR) analysis of ROR $\alpha$  (*Rora*), ROR $\gamma$ t (*Rorc*), and *Il17a* expression during T<sub>H</sub>17 cell development.  $\beta$ -actin was used as the internal control. **b** Western blot demonstrating protein expression of ROR $\gamma$ t and ROR $\alpha$  during T<sub>H</sub>17 cell development. Uncropped blots in Source Data. **c** FACS analysis of IL-17A and IL-17F expression in T cells transduced with empty vector (MIGR1), ROR $\alpha$ , or ROR $\gamma$ t. Cells were gated on live, GFP<sup>+</sup> cells. qRT-PCR analysis of ROR $\alpha$  and ROR $\gamma$ t expression from sorted GFP<sup>+</sup> cells (right) (**d**) qRT-PCR of sorted GFP<sup>+</sup> cells from Panel c.  $\beta$ -actin was used as the internal control. **e** FACS analysis of IL-17A vs IFN $\gamma$  expression (left panels) from T<sub>H</sub>17 cultures derived from *Rora*<sup>fl/fl</sup> (WT) and *Rora*<sup>fl/fl</sup> × *CD4*<sup>Cre</sup> (KO) mice. Graphs (middle panels) indicate percent IL-17A<sup>+</sup> cells in the cultures. FACS analysis (right panels) of ROR $\gamma$ t expression from a representative culture condition. **f** qRT-PCR of T<sub>H</sub>17-mediated cytokines in T<sub>H</sub>17 cell cultures from WT and KO mice.  $\beta$ -actin was used as the internal control. **g** Heat map of differentially expressed genes between WT and KO T<sub>H</sub>17 cells. KEGG pathway analysis of genes differentially expressed between WT and KO T<sub>H</sub>17 cells (FDR < 0.1). **h** (Top) Venn diagram depicting the numbers of unique and shared genes differentially regulated in WT/*Rora*<sup>fl/fl</sup> × *CD4*<sup>Cre</sup> and WT/ROR $\gamma$ <sup>-/-</sup> T<sub>H</sub>17 cells. Middle diagram shows the numbers of genes that are indirect or direct ROR $\alpha$  target genes in WT/*Rora*<sup>fl/fl</sup> × *CD4*<sup>Cre</sup> T<sub>H</sub>17 cells. Bottom diagram shows similar data for WT/ROR $\gamma$ <sup>-/-</sup> T<sub>H</sub>17 cells. A small number of direct target genes are shared between the two receptors (FDR < 0.1). Data are presented as mean values  $\pm$  s.e.m. ( $n = 3$ ). Student's two-tailed *t* tests were performed for statistical analysis. ns not significant ( $p > 0.05$ ). Source data are provided as a Source Data file.

decreased T<sub>H</sub>17 responses observed in ROR $\alpha$ -deficient T<sub>H</sub>17 cells. These data indicate that ROR $\alpha$  may regulate genes in diverse categories (i.e. ion transport, NADH metabolic processes, cell migration, etc.) that drive its function regulating cellular T<sub>H</sub>17 responses.

**ROR $\alpha$  is required for the development of chronic inflammatory diseases.** Recently, polymorphisms in *RORA* have been identified and associated with an increased risk for multiple sclerosis (MS)<sup>23</sup>. While found in non-coding regions, these SNPs were predicted to affect the affinity of transcription factor binding in regulatory regions of the *RORA* gene<sup>23</sup>. To establish how T-cell specific loss of ROR $\alpha$  affected autoimmune disease development, we immunized *Rora*<sup>fl/fl</sup> and *Rora*<sup>fl/fl</sup> × *CD4*<sup>Cre</sup> mice with MOG<sub>35–55</sub> peptide/complete freund's adjuvant (CFA) plus pertussis toxin to induce experimental autoimmune encephalomyelitis (EAE), a commonly used T<sub>H</sub>17-dependent mouse model of chronic-progressive MS<sup>24,25</sup>. While the incidence of disease between the two groups was not significantly different, *Rora*<sup>fl/fl</sup> × *CD4*<sup>Cre</sup> mice displayed attenuated disease severity relative to *Rora*<sup>fl/fl</sup> mice (Fig. 2a). Analysis of CD4<sup>+</sup> T cells from mice killed at the peak of disease (~Day 15) demonstrated a decreased percentage and number of CCR6<sup>+</sup> cells in the draining lymph nodes (LNs) and central nervous system (CNS) in the *Rora*<sup>fl/fl</sup> × *CD4*<sup>Cre</sup> mice (Fig. 2b and Supplementary Fig. 3). CCR6 is a chemokine receptor that permits T<sub>H</sub>17 cell migration into inflamed peripheral tissues, including the CNS and gut<sup>26</sup> and is thought to be a ROR $\gamma$ t target gene<sup>12</sup>. Genetic deletion or inhibition of CCR6 function has been shown to significantly reduce the severity of EAE<sup>27</sup>. Interestingly, there appeared to be an increase in the percent of CD25<sup>+</sup>Foxp3<sup>+</sup> cells in the LNs and CNS of *Rora*<sup>fl/fl</sup> × *CD4*<sup>Cre</sup> mice compared to *Rora*<sup>fl/fl</sup> control mice (Fig. 2c). This correlated with the decreased percent and number of ROR $\gamma$ t<sup>+</sup> cells in LNs and CNS (Fig. 2d). In line with this, there were significantly less IL-17A<sup>+</sup> cells, and importantly, significantly less IL-17A<sup>+</sup>IFN $\gamma$ <sup>+</sup> cells in *Rora*<sup>fl/fl</sup> × *CD4*<sup>Cre</sup> mice compared to *Rora*<sup>fl/fl</sup> control mice (Fig. 2e). IL-17A<sup>+</sup>IFN $\gamma$ <sup>+</sup> cells have been linked to pathogenicity in several models of chronic disease, including EAE/MS<sup>28–31</sup>. These data suggest that ROR $\alpha$  plays an important, non-redundant role to ROR $\gamma$ t in the development of EAE.

We next assessed whether loss of ROR $\alpha$  affects the development of colitis, another chronic inflammatory disorder associated with increased T<sub>H</sub>17 differentiation and function<sup>29,32</sup>. We sorted naive CD4<sup>+</sup> T cells from *Rora*<sup>fl/fl</sup> and *Rora*<sup>fl/fl</sup> × *CD4*<sup>Cre</sup> mice and transferred them (i.p.) into *Rag1*<sup>-/-</sup> recipients and monitored their weight over time. PBS/sham injected mice were used as a control. Mice receiving *Rora*<sup>fl/fl</sup> × *CD4*<sup>Cre</sup> T cells developed minimal signs of disease (weight loss, diarrhea, changes in colon length), unlike mice receiving *Rora*<sup>fl/fl</sup> naive CD4<sup>+</sup> T cells (Fig. 3a). Pro-inflammatory cytokine gene expression from proximal colons,

including *Il17a*, *Il17f*, *Il1b*, *Il6*, *Tnf*, *Ifng*, *Il22*, and *Il23p19*, was also significantly decreased in mice receiving *Rora*<sup>fl/fl</sup> × *CD4*<sup>Cre</sup> T cells compared to *Rora*<sup>fl/fl</sup> recipients (Fig. 3b). We also observed decreased expression of *Cxcl10*, a gene that is activated downstream of IL-17 and IL-22 signaling, which is consistent with the overall decreased T<sub>H</sub>17 proinflammatory profile observed in vivo. As expected, histological analysis revealed that mice receiving *Rora*<sup>fl/fl</sup> T cells developed more severe colitis, evidenced by the increased cellular infiltration, broadening of crypts, and epithelial hyperplasia (Fig. 3c). In contrast, mice receiving *Rora*<sup>fl/fl</sup> × *CD4*<sup>Cre</sup> T cells showed mild signs of inflammation in the proximal and distal colons. Analysis of mice at 6 weeks post-transfer indicated there were less *Rora*<sup>fl/fl</sup> × *CD4*<sup>Cre</sup> cells infiltrating the colon, likely due to *Rora*<sup>fl/fl</sup> × *CD4*<sup>Cre</sup> cells expressing significantly less  $\alpha$ 4 $\beta$ 7, an integrin that mediates lymphocyte extravasation to the intestinal lamina propria<sup>33</sup> (Fig. 3d, e). Similar to what was observed in the EAE model, *Rag1*<sup>-/-</sup> recipients receiving *Rora*<sup>fl/fl</sup> × *CD4*<sup>Cre</sup> cells showed an increase in the percent of CD25<sup>+</sup>Foxp3<sup>+</sup> cells in the mesenteric LNs (mLNs) and colons compared to mice receiving *Rora*<sup>fl/fl</sup> cells (Fig. 3f). Mice receiving *Rora*<sup>fl/fl</sup> × *CD4*<sup>Cre</sup> T cells also had significantly less ROR $\gamma$ t, IL-17A<sup>+</sup>, and IL-17A<sup>+</sup>IFN $\gamma$ <sup>+</sup> cells (Fig. 3g). Populations of T cells simultaneously expressing both cytokines have been described in intestinal biopsies of IBD patients<sup>34,35</sup>. Collectively, our genetic data suggests that ROR $\alpha$  plays a significant role in the development of T<sub>H</sub>17 cells, pathogenicity, and T<sub>H</sub>17-mediated pro-inflammatory diseases.

**ROR $\alpha$  controls T<sub>H</sub>17 cell responses through a cell intrinsic manner in vivo.** To address whether ROR $\alpha$  affects T<sub>H</sub>17 cell function through cell-intrinsic or cell-extrinsic mechanisms in vivo, we took advantage of a co-transfer model. We transferred equal numbers of congenic CD45.1<sup>+</sup> (WT) or CD45.2<sup>+</sup> ROR $\alpha$  KO (KO) naive CD4<sup>+</sup> T cells (i.p.) into *Rag1*<sup>-/-</sup> recipients (Fig. 4a). After 5 weeks of expansion, there was no observable difference in the ratio between WT and KO T cells in the spleen. However, there was a significant difference in the ratio of WT to KO T cells in the mLNs and colon lamina propria (LP) with WT markedly outcompeting KO T cells (Fig. 4a). Despite this phenotype observed in the spleen, we observed a decreased percentage of CCR6<sup>+</sup> cells in all KO T cells relative to WT in all tissues (spleen, mLNs, and colon LP; Fig. 4b). ROR $\alpha$  KO T cells also expressed significantly decreased amounts of ROR $\gamma$ t<sup>+</sup> cells as well as IL-17A<sup>+</sup> and IL-17A<sup>+</sup>IFN $\gamma$ <sup>+</sup> cells in mLN and colon LP relative to WT T cells (Fig. 4c, d). These results demonstrate that ROR $\alpha$  is required for T cell accumulation in the intestine and the downstream T<sub>H</sub>17 cell pro-inflammatory response. Furthermore, it cannot be rescued by the presence of ROR $\alpha$ -sufficient T cells. Therefore, ROR $\alpha$  activity in T<sub>H</sub>17 cells is required for their full effector function in vivo through a cell-intrinsic manner.

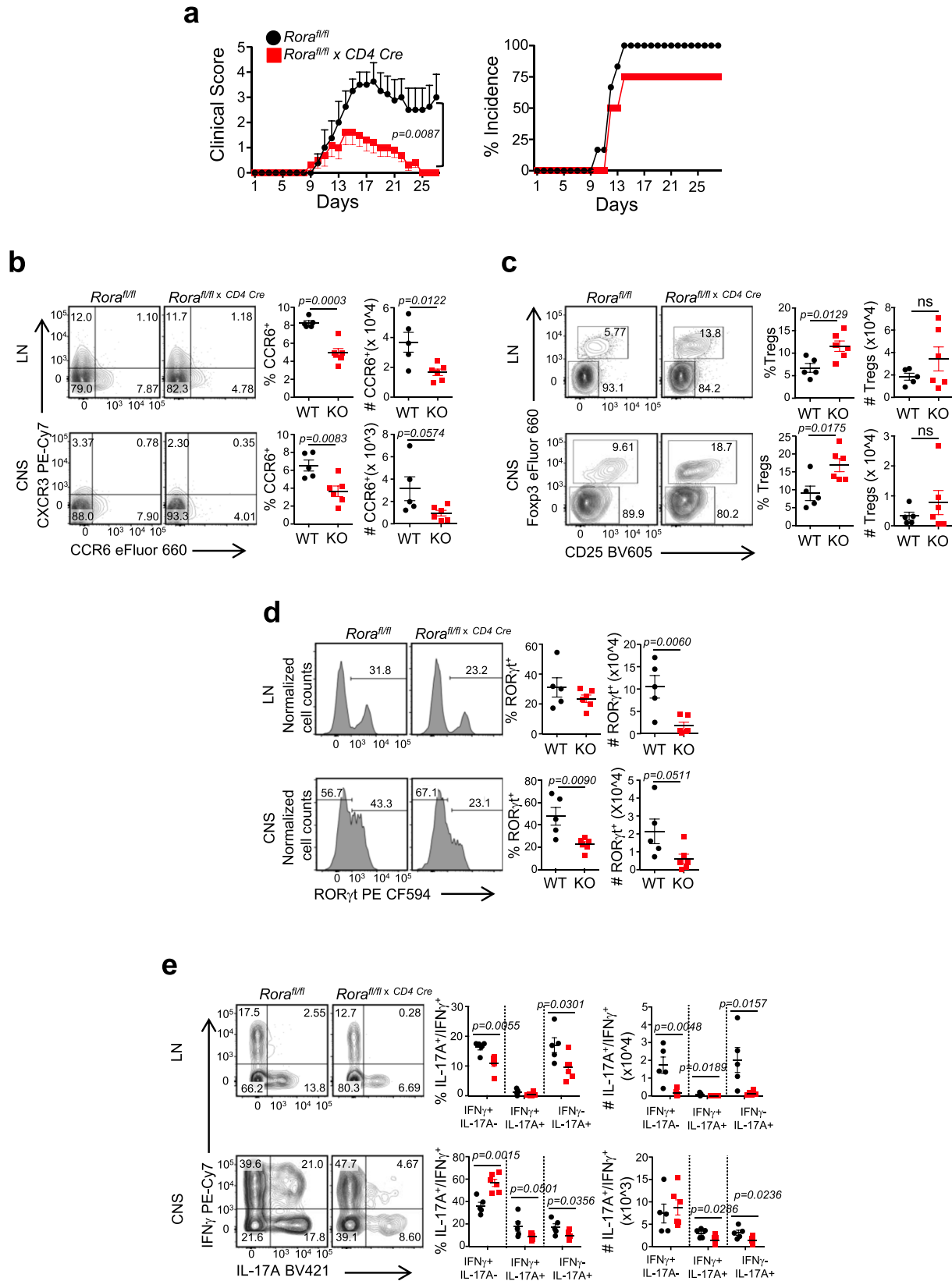


**Fig. 2 T-cell-specific loss of ROR $\alpha$  attenuates the severity of EAE.** **a** Clinical EAE scores (left) and disease incidence (right) from WT and KO mice subjected to MOG-induced EAE. Representative FACS plots and graphs (right) summarizing the frequency of **b** CCR6<sup>+</sup> and **c** CD25<sup>+</sup>Foxp3<sup>+</sup> T cells in the LN and CNS of WT vs. KO mice at the peak of disease. FACS analysis and graphs depicting the frequency and cell numbers of **d** ROR $\gamma$ t expression and **e** IL-17A<sup>+</sup>IFN $\gamma$ <sup>-</sup>, IL-17A<sup>+</sup>IFN $\gamma$ <sup>+</sup>, and IL-17A<sup>-</sup>IFN $\gamma$ <sup>+</sup> cells in the LN and CNS of WT and KO mice at the peak of disease. Cells were gated on live, CD45<sup>+</sup>CD3<sup>+</sup>CD4<sup>+</sup>CD44<sup>+</sup> cells. Each symbol represents an individual mouse [(WT, *n* = 5;  $\alpha$ KO, *n* = 6) for panels **a–e**]. Data are presented as mean values  $\pm$  s.e.m. Data are representative of two separate independent experiments generating similar results. Mann–Whitney *U* test for **a**, Student’s two-tailed *t* tests were performed for statistical analysis, **b–e**. Source data are provided as a Source Data file.

**A ROR $\alpha$ -selective small molecule regulates T<sub>H</sub>17 cell development.** We previously identified and characterized SR3335, a proof-of-concept ROR $\alpha$ -selective inverse agonist<sup>36</sup>. To date, SR3335 is the only ROR $\alpha$  inverse agonist in the primary literature that has been demonstrated to bind ROR $\alpha$  and modulate its activity<sup>36</sup>. When tested against all 48 human nuclear receptors, SR3335 exhibited modest activity at LXR $\beta$  and PXR, but this activity was negligible compared to full LXR and PXR agonists T0901317<sup>37</sup> and Rifampicin<sup>38</sup>, respectively (Supplementary Fig. 4A–C). To determine whether pharmacological modulation of ROR $\alpha$ 's activity can affect IL-17A expression, naïve CD4<sup>+</sup> T cells were differentiated under several T<sub>H</sub>17 conditions (non-pathogenic and pathogenic) in the presence of SR3335 or vehicle control. SR3335 dose dependently suppressed IL-17A expression without affecting cell viability (Fig. 5a). This effect was specific to ROR $\alpha$  and T<sub>H</sub>17 cells as the effect was lost when tested in *Rora*<sup>fl/fl</sup> × CD4<sup>Cre</sup> T<sub>H</sub>17 cells nor did SR3335 affect the development of T<sub>H</sub>1 or iTregs cells (Supplementary Fig. 4D, E). Gene expression analysis indicated that SR3335 inhibited the expression of *Il17a*, *Il17f*, *Il21*, *Il23r*, and *Ccr6* without affecting the expression of the LXR target gene *Abca1* (Fig. 5b). Since loss of ROR $\gamma$  and many recently developed ROR $\gamma$  modulators induce thymic apoptosis, we wanted to determine if genetic deletion and/or targeting ROR $\alpha$  induced similar effects. Unlike ROR $\gamma$ <sup>39</sup>, T-cell-specific deletion of ROR $\alpha$  had no effect on T cell development in the thymus (Fig. 5c, upper panels). To determine if SR3335 had any effects on thymic apoptosis, we treated C57BL/6 mice for 3 days with SR3335 (30 mg/kg, b.i.d, i.p.), the ROR $\gamma$ -selective inverse agonist SR2211<sup>40</sup> (20 mg/kg, b.i.d, i.p.), or vehicle controls. After 3 days, mice were killed to collect thymi to assess T cell development and total thymic cell numbers. Unlike mice treated with SR2211, which demonstrated decreased overall thymic cell number, percent of cells in the double positive stage, and total number of cells in the double positive stage, mice treated with SR3335 resembled vehicle control treated mice, indicating SR3335 had little effect on the thymus (Fig. 3c, lower panels). These data indicate that ROR $\alpha$ -selective inverse agonists can effectively target the T<sub>H</sub>17 pathway in vitro but do not appear to carry the associated risks of thymic apoptosis that ROR $\gamma$  inverse agonists do.

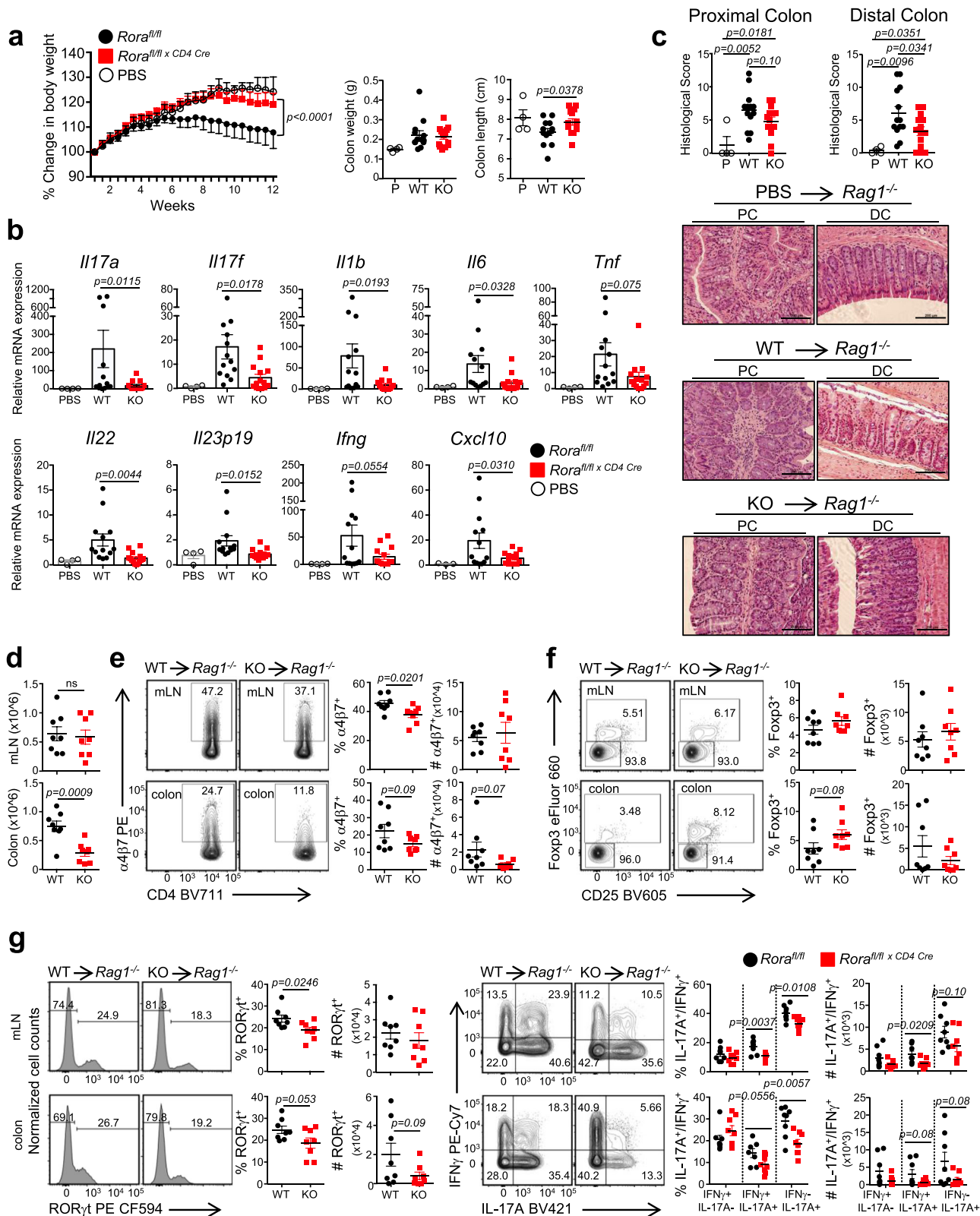
**SR3335 inhibits the development of autoimmunity.** To establish whether SR3335 was effective at inhibiting the development of autoimmunity in vivo, we immunized C57BL/6 mice to induce EAE and treated them with SR3335 (i.p. 30 mg/kg, B.I.D.) or vehicle control following immunization for the duration of the experiment. Dosing was based on drug metabolism and pharmacokinetic experiments performed in-house (Supplementary Fig. 5A). Disease development and incidence was delayed and significantly reduced in SR3335-treated animals relative to vehicle controls (Fig. 6a). Weights of the animals indicated no overt toxicity of the drug. Analysis of CD4<sup>+</sup> T cells at the peak of disease indicated a significantly decreased frequency of CD3<sup>+</sup> CD4<sup>+</sup> T cells in the CNS whereas the numbers of cells were decreased in the LNs and the CNS (Fig. 6b). The decreased frequency and number of cells in the CNS was likely due to the decreased percent of CCR6<sup>+</sup> cells in the CNS (Fig. 6c). SR3335 treatment led to a significant decrease in the frequency and number of ROR $\gamma$ <sup>+</sup> cells in the LNs and CNS (Fig. 6d). This correlated with the decreased frequency and number of GM-CSF<sup>+</sup> and IL-17A<sup>+</sup> cells in the LNs and CNS (Fig. 6e, f). GM-CSF-expressing T<sub>H</sub>17 cells have been shown to be highly encephalitogenic<sup>41,42</sup> (Fig. 6e). While there was only a very small difference in the frequency of IL-17A<sup>+</sup>IFN $\gamma$ <sup>+</sup> cells in the SR3335-

treated mice, the absolute numbers of these cells were significantly lower in the CNS of the drug-treated mice compared to vehicle controls (Fig. 6f). These data suggest that treatment with a ROR $\alpha$ -selective ligand largely phenocopy's the genetic data and is effective at inhibiting the development of autoimmunity.

**ROR $\alpha$ -selective ligands are inhibitory during active inflammation.** To evaluate whether SR3335 was effective during active inflammation we tested SR3335 in the PLP<sub>139-151</sub>-induced relapsing-remitting EAE (R-EAE) model. SR3335 (30 mg/kg, B.I.D.) or vehicle was administered once mice had recovered from the first wave of disease (day 18 post-immunization). SR3335 significantly reduced the relapse rate and severity of relapse compared to animals receiving vehicle (Fig. 7a). Similar to the chronic EAE model, SR3335 appeared to inhibit cellular infiltration into the CNS, indicated by the decreased number of cells in the CNS relative to the draining lymph nodes (Fig. 7b). This was likely due to the decreased expression of CCR6 on CD4<sup>+</sup> T cells (Fig. 7c). Intracellular FACS analysis demonstrated a decreased frequency and number of ROR $\gamma$ <sup>+</sup> cells in the LNs and CNS of the SR3335-treated mice relative to vehicle controls (Fig. 7d). While we did observe a small decrease in IL-17A expression in the LNs of these mice, we did not observe a difference in the frequency of ROR $\gamma$ <sup>+</sup>IL-17A expression in the CNS of vehicle versus SR3335-treated mice. However, there was a significant reduction of the number of IL-17A<sup>+</sup> and pathogenic IL-17A<sup>+</sup>IFN $\gamma$ <sup>+</sup> cells in CNS compared to mice receiving vehicle control (Fig. 7e). These results offer proof-of-concept that pharmacological modulation of ROR $\alpha$  activity post-disease onset (therapeutic mode) can suppress the progression of T<sub>H</sub>17-driven autoimmunity and chronic inflammatory disorders.

**SR3335 regulates memory T<sub>H</sub>17 and T<sub>H</sub>17.1 cells.** It has been difficult to differentiate naïve human CD4<sup>+</sup> T cells into T<sub>H</sub>17 cells that secrete a substantial amount of IL-17A. However, recent work has demonstrated that anti-CD3 stimulation in the presence of IL-23 and IL-1 $\beta$ , without anti-CD28, is sufficient to drive an abundant IL-17 response in human T cells<sup>43</sup>. To determine if SR3335 was effective at inhibiting human T<sub>H</sub>17 cell differentiation, we isolated human naïve CD4<sup>+</sup> T cells from peripheral blood mononuclear cells (PBMCs) and differentiated them under conditions described by Revu et al.<sup>43</sup>. Similar to mouse T<sub>H</sub>17 cells, SR3335 dose dependently inhibited the development of human T<sub>H</sub>17 cells without affecting cell viability (Fig. 8a). To establish whether inhibition of ROR $\alpha$  activity would affect T<sub>H</sub>17 cells derived from patients with IBD, specifically Ulcerative Colitis (UC), we differentiated naïve CD4<sup>+</sup> T cells from PBMCs from UC patients vs. healthy, age-matched controls (HC) under conditions described in Fig. 8a. While PBMCs from UC patients consistently yielded greater amounts of IL-17A and IFN $\gamma$ , SR3335 was still able to inhibit IL-17A in a dose dependent manner (Supplementary Fig. 5b).

IL-17A expressing memory cells (CD45RO<sup>+</sup>) are enriched within PBMCs and can be identified by their co-expression of CCR6 and CCR4<sup>44</sup>. However, CCR6<sup>+</sup> human memory cells can be further subdivided based on expression of CXCR3, which describes a subset of cells that expresses both IL-17A and IFN $\gamma$  upon ex-vivo stimulation<sup>45</sup>. These two populations of cells have been demonstrated to be stable and are referred to as T<sub>H</sub>17 (CCR6<sup>+</sup>CCR4<sup>hi</sup>CXCR3<sup>lo</sup>) and T<sub>H</sub>17.1 (CCR6<sup>+</sup>CCR4<sup>lo</sup>CXCR3<sup>hi</sup>)<sup>46,47</sup>. To determine whether SR3335 could affect IL-17A expression in human memory T<sub>H</sub>17 subsets, we sorted memory T helper cell subsets based on expression of CCR6, CCR4, and CXCR3 to isolate memory T<sub>H</sub>1, T<sub>H</sub>2, T<sub>H</sub>17, and T<sub>H</sub>17.1 populations. (All populations were CD4<sup>+</sup>CD45RO<sup>+</sup>CD25<sup>-</sup>CRTH2<sup>-</sup>CCR10<sup>-</sup>.) Sorted



populations were cultured for 6 days in the presence of vehicle or SR3335, after which time cells were FACS analyzed to determine intracellular cytokine profiles. Consistent with the mouse in vitro cultures, SR3335 had little effect on the T<sub>H</sub>1 (CCR6<sup>-</sup>CCR4<sup>lo</sup>CXCR3<sup>hi</sup>) and T<sub>H</sub>2 (CCR6<sup>-</sup>CCR4<sup>hi</sup>CXCR3<sup>lo</sup>) cultures (Fig. 8b). However, SR3335 significantly inhibited the expression of IL-17A in the human memory T<sub>H</sub>17 cultures but did not quite

reach significance in the T<sub>H</sub>17.1 cultures. Treatment with SR3335 also led to a small but reproducible increase in expression of IL-22 (Fig. 8c) while inhibiting TNFα expression in T<sub>H</sub>17 and T<sub>H</sub>17.1 populations, without affecting TNFα expression in T<sub>H</sub>1 or T<sub>H</sub>2 memory populations (Fig. 8d, e). This SR3335-mediated increase in IL-22 extends to mouse memory cells as culture of sorted mouse CCR6<sup>+</sup> cells treated with SR3335 induced a similar response

**Fig. 3 ROR $\alpha$ -deficient T cells protect from the development of colitis.** **a** Percent change in body weight, colon weights, and colon lengths of *Rag1*<sup>-/-</sup> recipient mice over 12 weeks post-adoptive transfer of *Rora*<sup>fl/fl</sup> (WT), *Rora*<sup>fl/fl</sup> × *CD4*<sup>Cre</sup> (KO), or control (no cells, PBS) T cells. **b** qRT-PCR analysis of cytokines expressed in the proximal colon from *Rag1*<sup>-/-</sup> mice receiving PBS, *Rora*<sup>fl/fl</sup> (WT), or *Rora*<sup>fl/fl</sup> × *CD4*<sup>Cre</sup> (KO) CD4<sup>+</sup> T cells. 18 s was used as the internal control. **c** Histology scores from proximal and distal colons from *Rag1*<sup>-/-</sup> mice receiving PBS, *Rora*<sup>fl/fl</sup> (WT), or *Rora*<sup>fl/fl</sup> × *CD4*<sup>Cre</sup> (KO) CD4<sup>+</sup> T cells (top graphs). Representative hematoxylin and eosin stained sections from proximal and distal colons from the same mice 12 weeks post T-cell transfer (×20 magnification, scale bars 200  $\mu$ m). [*n* = 4 (PBS), *n* = 13 (WT), and *n* = 14 (KO) for panels **a-c**]. **d** Cell counts from mesenteric lymph nodes (mLN) and colons of mice receiving WT and KO T cells at 6 weeks post-transfer. Representative FACS plots and graphs (right) summarizing the frequency and cell numbers of **e**  $\alpha$ 4 $\beta$ 7<sup>+</sup> and **f** CD25<sup>+</sup>Foxp3<sup>+</sup> T cells in the mLN and colons of WT vs KO mice at 6 weeks post-transfer. **g** FACS analysis and graphs depicting the frequency and cell numbers of ROR $\gamma$ t expression (left) and IL-17A<sup>+</sup>IFN $\gamma$ <sup>-</sup>, IL-17A<sup>+</sup>IFN $\gamma$ <sup>+</sup>, and IL-17A<sup>-</sup>IFN $\gamma$ <sup>+</sup> cells in the mLN and colons of WT and KO mice at 6 weeks post-transfer. Cells were gated on live, CD45<sup>+</sup>CD3<sup>+</sup>CD4<sup>+</sup>CD44<sup>+</sup> cells. Each symbol represents an individual mouse [*n* = 8 (WT), *n* = 8 (KO) for panels **e-g**]. Data are presented as mean values  $\pm$  s.e.m. Data are representative of two combined independent experiments. Mann-Whitney *U* test for **a**, Student's two-tailed *t* tests were performed for statistical analysis, **b-g**. Source data are provided as a Source Data file.

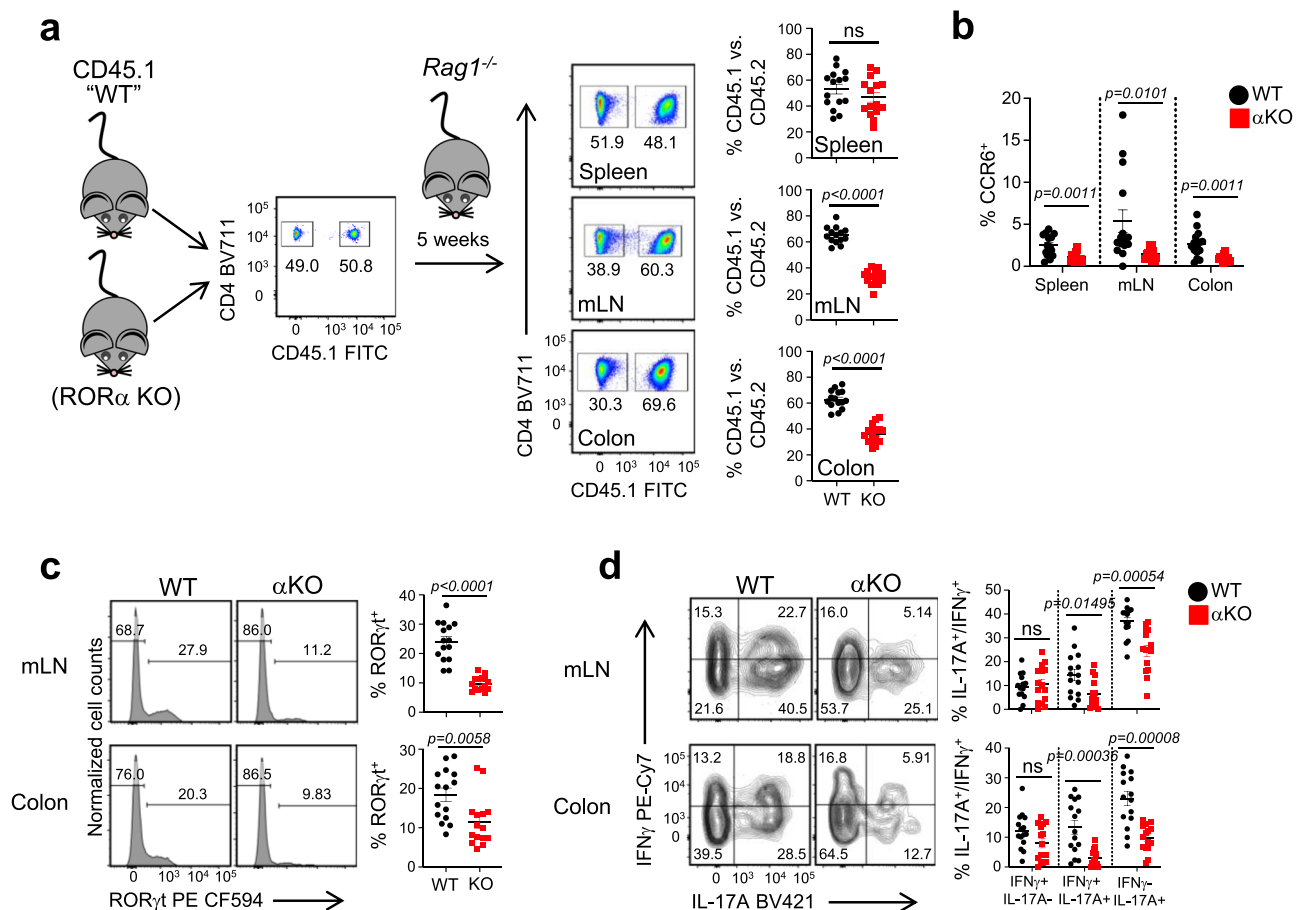


**Fig. 4 Defects in ROR $\alpha$ -deficient T cells in colitis is cell intrinsic.** **a** Schematic of experimental set up. Naïve CD4<sup>+</sup> T cell were sorted from CD45.1 (WT) and ROR $\alpha$  T cell deficient ( $\alpha$ KO) mice and transferred into *Rag1*<sup>-/-</sup> recipient mice. Representative FACS plot from one experiment (left panel). Right panels; representative FACS plots and graphs demonstrating the frequency of WT vs.  $\alpha$ KO T cells present in the spleens, mLNs, and colons of *Rag1*<sup>-/-</sup> recipient mice 5 weeks post-transfer. **b** Graphs summarizing the frequency of CCR6<sup>+</sup> cells in each tissue. FACS analysis and graphs depicting the frequency of **c** ROR $\gamma$ t expression and **d** IL-17A<sup>+</sup>IFN $\gamma$ <sup>-</sup>, IL-17A<sup>+</sup>IFN $\gamma$ <sup>+</sup>, and IL-17A<sup>-</sup>IFN $\gamma$ <sup>+</sup> cells in the mLN and colons of WT and  $\alpha$ KO mice at 5 weeks post-transfer. Cells were gated on live, CD3<sup>+</sup>CD44<sup>+</sup>CD4<sup>+</sup> and CC45<sup>+</sup> or CD45<sup>-</sup> cells. Each symbol represents an individual mouse [*n* = 15 (WT), *n* = 15 ( $\alpha$ KO) for panels **a-d**]. Data are presented as mean values  $\pm$  s.e.m. Data are representative of two combined independent experiments. Student's two-tailed *t* tests were performed for statistical analysis. Source data are provided as a Source Data file.

(Supplementary Fig. 5C). Gene expression analysis from these samples revealed that SR3335 inhibited expression of many “core” T<sub>H</sub>17 genes, including *IL17A*, *IL17F*, *CCR6*, and *IL12RB1*, which was consistent with much of the mouse data (Fig. 8f). Interestingly, SR3335 treatment also led to an increase in the transcription factor *MAF* in T<sub>H</sub>17 and T<sub>H</sub>17.1 populations. Collectively, these results indicate that ROR $\alpha$ -selective inverse agonists can inhibit T<sub>H</sub>17 cell

functions in lineage-committed human memory T cells as well as from patients with T<sub>H</sub>17 inflammatory diseases, like UC.

## Discussion

Here we used a combination of genetic, molecular biology, and pharmacological approaches to demonstrate that ROR $\alpha$  is a



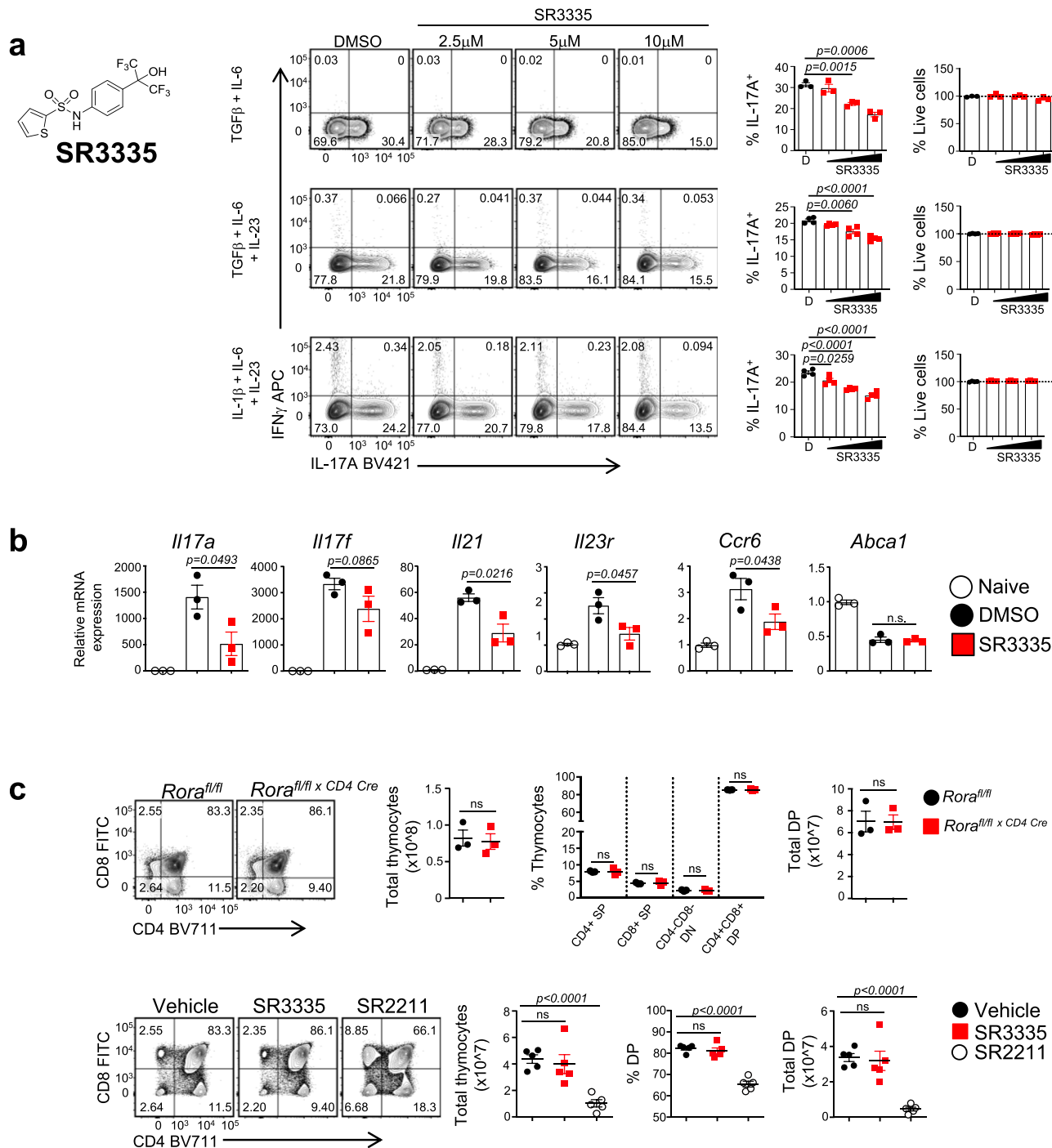
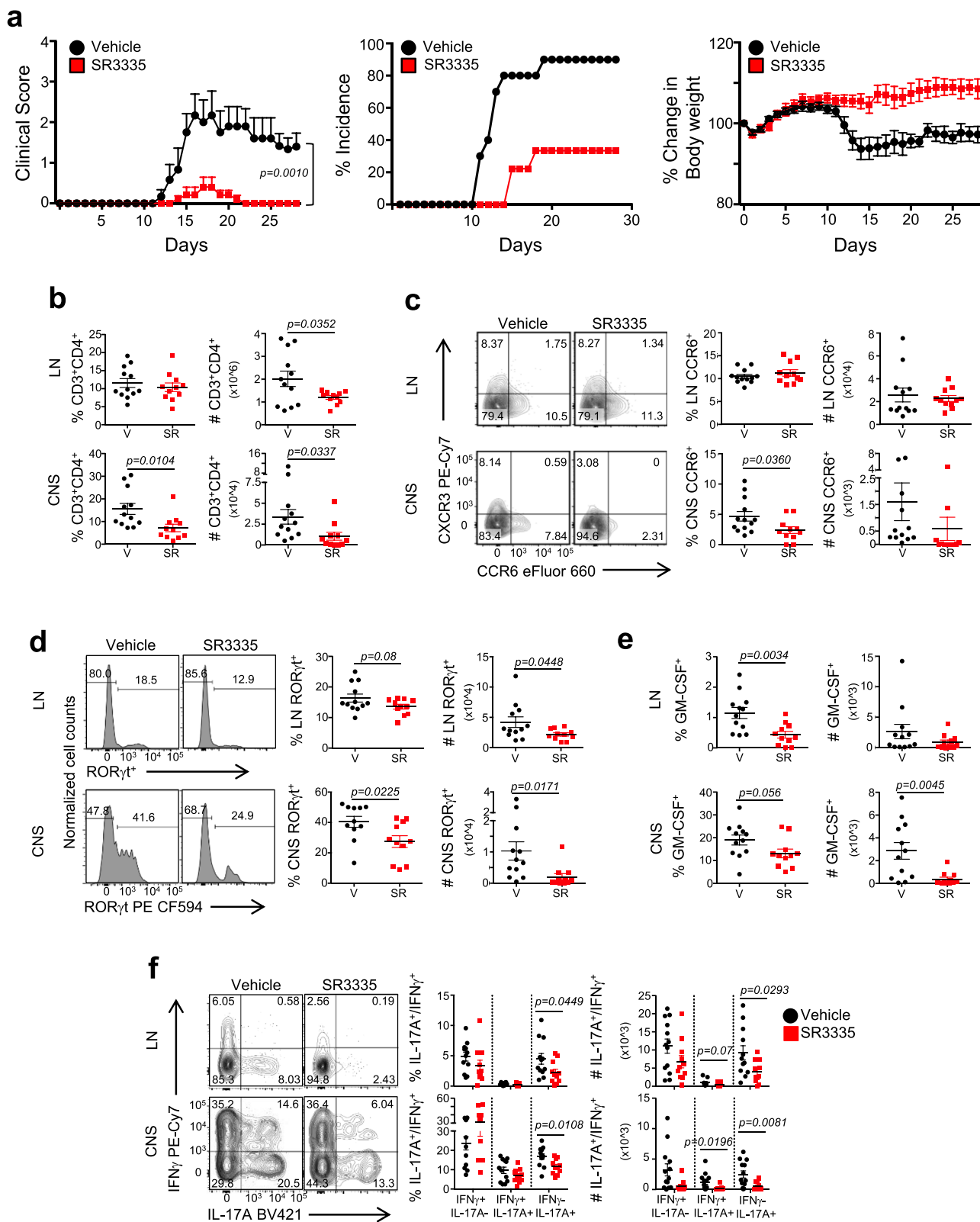


**Fig. 5 ROR $\alpha$ -specific small molecule suppresses T<sub>H</sub>17-cell development.** **a** Mouse naïve CD4<sup>+</sup> T cells were differentiated under three different T<sub>H</sub>17 polarizing conditions (non-pathogenic and pathogenic) and treated with vehicle (DMSO) or SR3335. IL-17A and IFN $\gamma$  expression were analyzed by flow cytometry. Graphs indicate percent IL-17A<sup>+</sup> cells and frequency of live cells in cultures with compound treatment. **b** qRT-PCR of T<sub>H</sub>17-mediated cytokines in cells treated with vehicle (DMSO) or SR3335 (5μM). Analysis was performed at 96 h post T-cell activation and compared to naïve CD4<sup>+</sup> T cells.  $\beta$ -actin was used as the internal control.  $n = 3$  technical replicates. **c** FACS analysis of thymocytes from 8-week-old *Rora*<sup>fl/fl</sup> (WT) or *Rora*<sup>fl/fl</sup> × *CD4*<sup>Cre</sup> (KO) mice (top panels). Graphs demonstrate the total thymocyte number, frequency of thymocytes per subset, and total double positive (DP) cell number. (SP single positive, DP double positive, DN double negative;  $n = 3$ /group). (bottom panels) FACS analysis of mice treated with vehicle, SR2211, or SR3335 for 72 h. Graphs depict total thymocyte number, percent of double positive cells, and number of double positive cells in each group. Data are presented as mean values  $\pm$  s.e.m. Data shown are representative of two separate, independent experiments ( $n = 5$ /group). Student's two-tailed  $t$  tests were performed for statistical analysis, ns not significant ( $p > 0.05$ ). Source data are provided as a Source Data file.



major regulator of T<sub>H</sub>17 cell development, autoimmunity, and chronic inflammation. We demonstrated that in vitro, despite equal amounts of ROR $\gamma$ t in cells, loss of ROR $\alpha$  leads to a reduction in IL-17A expression, with no effect on the development of other T helper cell populations, including Foxp3<sup>+</sup> T regulatory cells. Using mouse models of EAE and colitis we show that loss of ROR $\alpha$  affected the expression of IL-17A, ROR $\gamma$ t, as

well as the frequency of CD25<sup>+</sup>Foxp3<sup>+</sup> Tregs in vivo. Pharmacological studies demonstrated that use of a ROR $\alpha$ -selective inverse agonist, SR3335, inhibited the development of mouse T<sub>H</sub>17 cells in vitro and in vivo, while leaving thymic T cell development intact, unlike ROR $\gamma$  modulators. Importantly, we determined that SR3335 effectively inhibits human T<sub>H</sub>17 cells as well.

**Fig. 6 SR3335 suppresses the development and severity of chronic EAE.** **a** Clinical EAE scores (left) from mice subjected to MOG-induced EAE and treated with Vehicle (10/10/80 formulation of DMSO/Tween80/H<sub>2</sub>O) or SR3335 (i.p., 30 mg/kg, b.i.d.) for the duration of the experiment. Middle graph demonstrates the percent incidence of disease. Right graph demonstrates the percent change in body weight over time between the two groups. (Vehicle,  $n = 10$ ; SR3335,  $n = 10$ ) Data representative of three separate, independent experiments with similar results. **b** Frequencies and cell number of CD3<sup>+</sup>CD4<sup>+</sup> cells in the draining lymph nodes (LN) and CNS of mice at peak of disease. **c** Representative FACS plots and graphs (right) summarizing the frequency and cell number of CCR6<sup>+</sup> and T cells in the LNs and CNS of vehicle vs. drug treated mice at the peak of disease. **d** FACS analysis, frequencies, and cell counts of RORγt<sup>+</sup> cells in LNs and CNS of mice at peak of disease. **e** Graphs depicting the frequencies and cell counts of CD4<sup>+</sup>GM-CSF<sup>+</sup> cells in LN and CNS of mice at peak of disease. **f** FACS analysis, frequencies, and cell counts of IL-17A<sup>+</sup>IFNγ<sup>-</sup>, IL-17A<sup>+</sup>IFNγ<sup>+</sup>, and IL-17A<sup>-</sup>IFNγ<sup>+</sup> cells in the LN and CNS of mice at the peak of disease. Cells were gated on live, CD45<sup>+</sup>CD3<sup>+</sup>CD4<sup>+</sup>CD44<sup>+</sup> cells. [V = Vehicle ( $n = 12$ ), SR = SR3335-treated mice ( $n = 11$ ) for panels **b-f**]. Data are presented as mean values ± s.e.m. Data are representative of two combined independent experiments with similar results. Mann-Whitney *U* test for **a**, Student's two-tailed *t* tests were performed for statistical analysis, **b-f**. Source data are provided as a Source Data file.

Despite its clear effects and synergism with RORγt on T<sub>H</sub>17 cell development<sup>8</sup>, the functional role of RORα was never expanded upon. Importantly, the T-cell specific role of RORα or its effects in other models of chronic inflammation were never explored because RORα was considered “redundant” to RORγt. In nuclear receptor research, there are many receptor sub-families where one member is considered “dominant” and the other “redundant.” However, recent studies have started to tease apart the distinct signaling pathways for receptors in these sub-families demonstrating that they each possess a unique, requisite function in each cell type. For example, RXRα (NR2B1) and RXRβ (NR2B2) were recently shown to have distinct functions in retinoic acid signaling and neuronal differentiation<sup>48</sup>. Both LXRA (NR1H2) and LXRβ (NR1H3) were each found selectively associated with sequence motifs of specific transcription factors demonstrating LXRA- or LXRβ-selective gene regulation in macrophages<sup>49</sup>. Since redundancy suggests dispensable or unnecessary, our data indicates that RORα is a requisite factor for T<sub>H</sub>17 cell differentiation and the development of autoimmunity. Indeed, a recent publication has hinted at RORα's function in T<sub>H</sub>17 cell pathogenicity in a *Rip2*-dependent fashion. In this report, *Rip2* negatively regulated the expression of RORα as *Rip2*<sup>-/-</sup> CD4<sup>+</sup> T cells expressed more RORα than WT CD4<sup>+</sup> T cells<sup>50</sup>. The authors reported that RORα drove the expression of *Il1r1*, which they determined was RORα-dependent and was the basis for enhanced T<sub>H</sub>17 cell pathogenicity. While the increase in IL-1β signaling is consistent with increased pathogenicity observed in T<sub>H</sub>17 cells<sup>51,52</sup>, our data analysis has determined that *Il1r1* is regulated by both RORα and RORγt. Nevertheless, it still needs to be determined how and why *Rip2* is regulating RORα expression in T<sub>H</sub>17 cells and what the biological significance of this is. Our genomics analysis did, however, identify some unique direct RORα target genes, including those that are important for mitochondrial metabolism (*Idh3a*, *Gpd2*, and *Ndufb2*), ion transport (*Slc11a2*), and other T<sub>H</sub>17 cell transcriptional regulators (*Fosl2*), underscoring the need to further probe the function of this transcription factor. What is interesting to note is that numerous genes, like *Ccr6*, *Il17a*, *Il23r*, did not appear to be direct RORα target genes. This is likely a function of the cell type used for ChIP-seq analysis and further analysis assessing RORα's cis-trome in T<sub>H</sub>17 cells is warranted to understand its full regulatory functions.

Interestingly, deletion of RORα increased Treg frequencies in vivo. However, treatment with SR3335 trended towards an increase, but did not significantly phenocopy the knock out mice. This may be due, in part, to the pharmacokinetic properties of SR3335 in vivo. The  $K_i$  of SR3335 was reported as 220 nM with an IC<sub>50</sub> of 480 nM in a Gal4-RORα ligand binding domain cotransfection assay<sup>36</sup>. With the plasma exposure at 230 nM at 6 h and falling quickly thereafter, the activity on target is likely not 100% throughout a 24-h period, even with B.I.D. dosing. Perhaps use of a more potent inverse agonist, with better in vivo exposure,

would generate a more significant response and phenocopy the genetic models. Alternatively, a complete deletion of RORα may be necessary to observe the phenotype as changes in chromatin structure are likely to happen in the absence of a gene more so than through pharmacological modification. Regardless, RORα has been demonstrated to be expressed in skin-resident Tregs and its expression is required to restrain allergic skin inflammation<sup>53</sup>. Acquisition of RORα expression appears to occur once the cells are in the skin as RORα expression is low in skin draining lymph nodes<sup>53</sup>. This is intriguing given a previous report described an antagonistic role for Foxp3 in RORα-mediated gene transcription. In this scenario, Foxp3, via its LXXLL domain, directly interacted with RORα to inhibit *Il17a* transcription<sup>10</sup>. While some of the genes differentially expressed in skin-resident RORα-expressing Tregs are similar to those in RORα-deficient T<sub>H</sub>17 cells (*Ccr6*, *Cd44*, *Nr1d1*, etc.), perhaps this molecular antagonism between RORα and Foxp3 may not occur in skin-resident Tregs, or only at select target genes. Based on the increased frequencies of Tregs in RORα-deficient mice with EAE and colitis, this molecular antagonism might occur at sites with different inflammatory stimuli than in the skin. A similar cooperativity has been described for RORγt and STAT3 in the differentiation of T<sub>H</sub>17 vs. Tregs<sup>11</sup>. In the absence of pro-inflammatory cytokines, TGFβ-mediated Foxp3 induction drives Tregs by inhibiting RORγt. However, in the presence of pro-inflammatory cytokines, including IL-6, RORγt is stabilized, promoting T<sub>H</sub>17 differentiation<sup>11</sup>. RORγt-deficient mice have increased Foxp3<sup>+</sup> Tregs<sup>7</sup> and are protected from EAE, similar to what we observe in RORα-deficient T cells. It is possible that a similar mechanism occurs between RORα and Foxp3 in the regulation of T<sub>H</sub>17 vs. Treg development, or cooperation occurs between all three transcription factors. However, further in-depth studies are required to understand how RORα may be regulating the T<sub>H</sub>17/Treg balance.

RORα appears to regulate the expression of several genes important for T<sub>H</sub>17 cell migration and function, specifically CCR6<sup>26</sup>. Decreased expression of CCR6 may underlie the decreased number of cells observed in inflamed sites, including the colon and CNS. While CCR6 is classically considered a RORγt target gene<sup>12</sup>, its expression was significantly decreased in vitro and in vivo in RORα-deficient or SR3335-treated T cells. While this may be a consequence of decreased RORγt expression, we do not believe this to be the case because in vitro, protein expression of RORγt present between wild-type and RORα-deficient T<sub>H</sub>17 cells was similar (Fig. 1e). These data would suggest that CCR6 is either a shared target gene with RORγt or, relies on RORα for expression. While *Ccr6* did not appear to be a direct RORα target gene in our analysis, again this could be due to the tissue type analyzed. Interestingly, expression of *Ccr6* is altered in RORα<sup>-/-</sup> skin Tregs<sup>53</sup>, so we believe the latter is the case. The situation with IL-17A is a little more complicated. It too is decreased in vivo and one could argue that its decreased expression is a function of decreased RORγt expression. However,

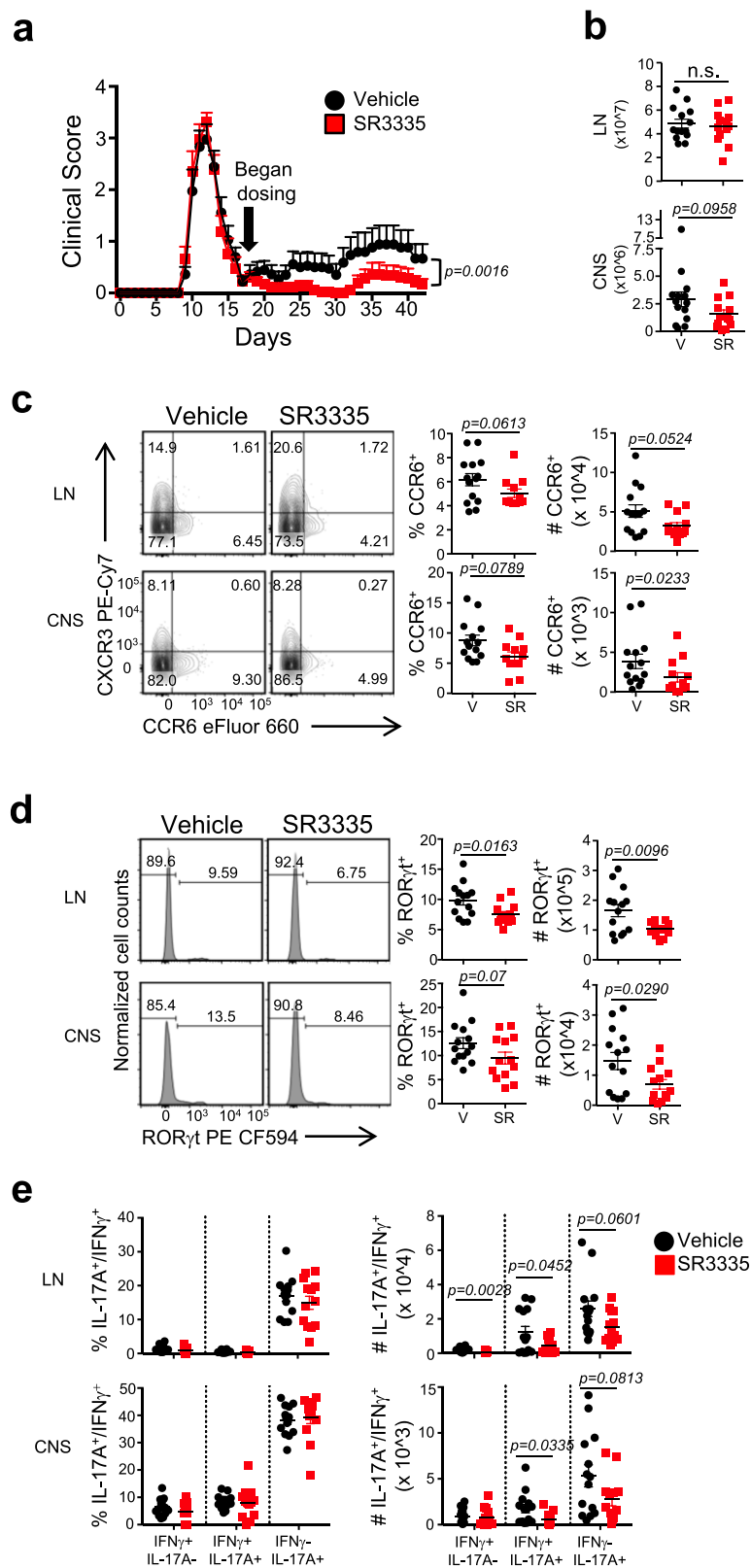


**Fig. 7** SR3335 is effective when used therapeutically in relapsing-remitting EAE. **a** Clinical EAE scores of mice from relapsing-remitting model of EAE treated with vehicle or SR3335 (i.p., 30 mg/kg, b.i.d.) starting on day 18 and continued for the duration of the experiment ( $n = 18$ /group). Data are representative of two separate experiments. **b** Cell counts from draining lymph nodes (LN) and CNS of mice at the termination of the experiment. FACS plots, frequencies and cell counts of **c** CCR6<sup>+</sup> and **d** ROR $\gamma$ t<sup>+</sup> T cells in the LNs and CNS of vehicle and SR3335-treated mice. **e** Graphs representing the frequencies and cell counts of IL-17A<sup>+</sup>IFN $\gamma$ <sup>-</sup>, IL-17A<sup>+</sup>IFN $\gamma$ <sup>+</sup>, and IL-17A<sup>-</sup>IFN $\gamma$ <sup>+</sup> cells in the LNs and CNS of mice treated with vehicle and SR3335. [ $n = 14$ , vehicle;  $n = 13$ , SR3335) for panels **c–e**]. Data are presented as mean values  $\pm$  s.e.m. Data are representative of two combined independent experiments with similar results. Mann-Whitney  $U$  test for **a**, Student's two-tailed  $t$  tests were performed for statistical analysis, **b–e**. Source data are provided as a Source Data file.

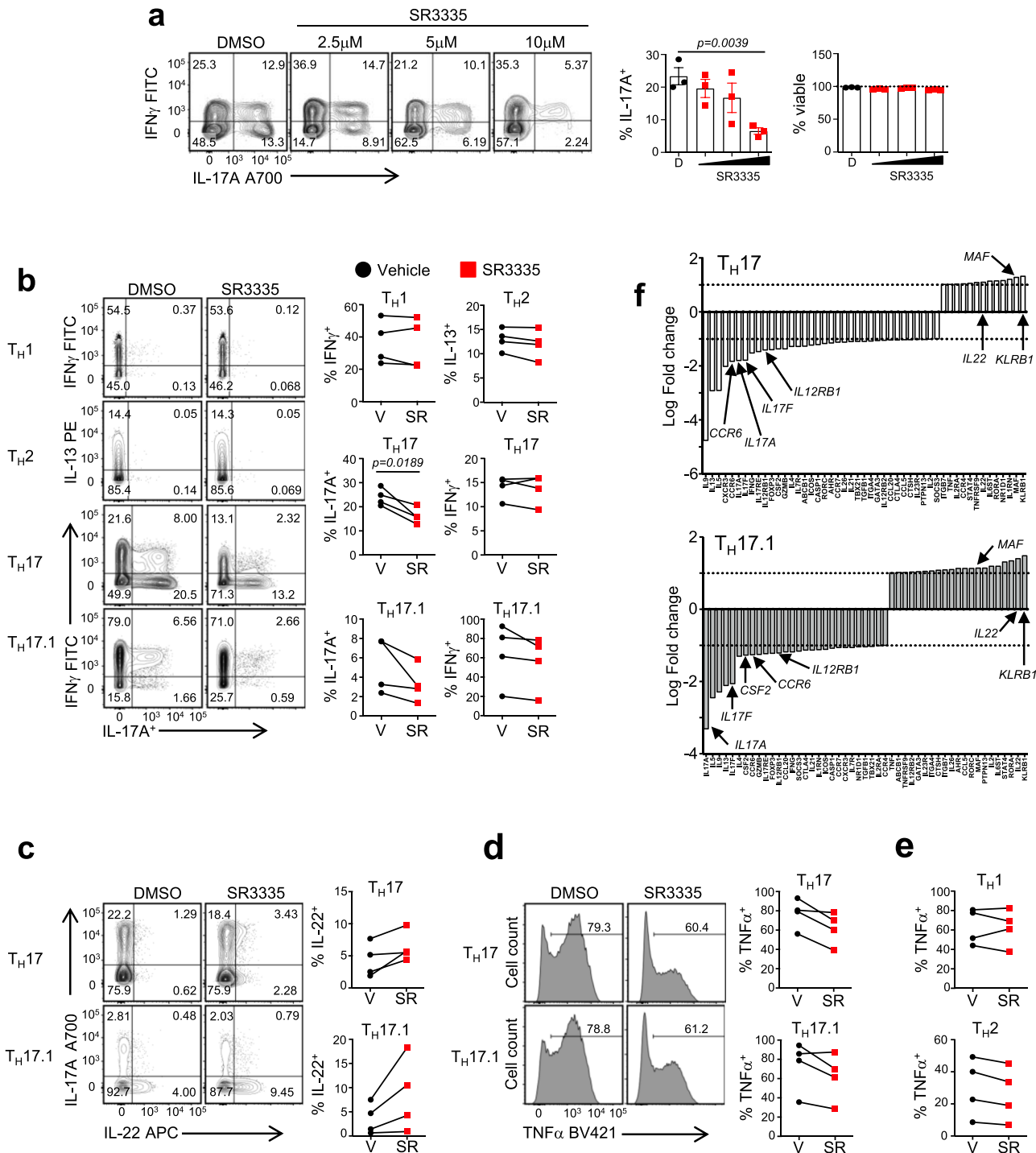


**Fig. 8 SR3335 modulates human memory T<sub>H17</sub> and T<sub>H17.1</sub> cells.** **a** Naive human CD4<sup>+</sup> T cells were differentiated under T<sub>H17</sub> polarizing conditions (anti-CD3 + IL-23+IL-1 $\beta$ ) and treated with vehicle (DMSO) or SR3335. IL-17A and IFN $\gamma$  expression were analyzed from live, CD45RO<sup>+</sup> cells by flow cytometry on Day 6. Graphs indicate percent IL-17A<sup>+</sup> cells and frequency of live cells in cultures with compound treatment. **b** FACS sorted memory cell (CD4<sup>+</sup>CD25<sup>-</sup>CD45RO<sup>+</sup>) subsets from healthy adult donor peripheral blood were stimulated with PMA and ionomycin in the presence of vehicle (V, DMSO) or SR3335 (SR, 5 $\mu$ M). Graphs depict percentage cytokine production by flow cytometry after 6 days in culture. **c** FACS analysis of T<sub>H17</sub> and T<sub>H17.1</sub> sorted memory cells to determine IL-17A and IL-22 expression and **d** TNF $\alpha$  expression. **e** Graphs summarizing the percentage TNF $\alpha$  expression in sorted T<sub>H1</sub> and T<sub>H2</sub> memory cells treated with vehicle (V, DMSO) or SR3335 (SR, 5  $\mu$ M) for 6 days from four different donors. **f** Nanostring data demonstrating the SR3335-mediated changes in gene expression in T<sub>H17</sub> and T<sub>H17.1</sub> cultures on day 6 from the combined data of three donors described in panel **e**. Data are presented as mean values  $\pm$  s.e.m. Student's two-tailed *t* tests were performed for statistical analysis. Source data are provided as a Source Data file.

IL-17A is also decreased *in vitro* despite equal amounts of ROR $\gamma$ t. The answer could lie with the fact that ROR $\gamma$ t is a member of the nuclear receptor superfamily and thus a ligand-regulated transcription factor. There have been several reports describing natural, endogenous ligands for ROR $\gamma$ t expressed in T<sub>H</sub>17 cells<sup>54–56</sup>. Therefore, expression of a receptor does not always correlate with activity. It is possible that ROR $\alpha$ -deficiency leads to dysregulation of pathways that invariably affect the production of endogenous ROR $\gamma$ -ligands. This would manifest as downstream changes in gene expression rather than expression of the receptor itself. Consequently, ROR $\alpha$  could affect T<sub>H</sub>17 cell development through mechanisms regulating cellular metabolic processes.

While initially characterized in a diet induced obese (DIO) mouse model of type 2 diabetes<sup>36</sup>, our efforts to examine SR3335's effects in mouse models of autoimmunity and chronic inflammation have demonstrated that it effectively and largely phenocopies much of the genetic effects observed in the *Rora*<sup>fl/fl</sup> × *CD4* *Cre* mice. We also found it interesting that SR3335 increased expression of IL-22 in both mouse and human memory T<sub>H</sub>17 cells whereas Nanostring analysis indicated that SR3335 increased the mRNA expression of both *MAF* and *IL22* in human memory T<sub>H</sub>17 and T<sub>H</sub>17.1 cells. This is confounding given that c-Maf has been demonstrated to inhibit IL-22 expression<sup>57</sup>. However, the change in gene expression is minor relative to protein expression via FACS. Given c-Maf's role in T cell effector function and cytokine expression has been well documented<sup>58–60</sup>, this needs to be interrogated further. This will be particularly important since production of IL-22 by T<sub>H</sub>17 cells has been shown to be upregulated during tissue injury to promote repair<sup>61</sup>. Thus, the observed increase in IL-22 production coupled with decreased IL-17A and TNF $\alpha$  with SR3335 highlight the benefits of targeting ROR $\alpha$  in chronic inflammatory diseases like IBD where such actions would prove beneficial to patients. Importantly, the effects on IL-22 appears to be specific to the ROR $\alpha$  ligand as other, previously published ROR $\gamma$  inverse agonists did not have similar effects<sup>14</sup>. In contrast to beneficial effects in IBD, SR3335 inhibited TNF $\alpha$  in T<sub>H</sub>17 and T<sub>H</sub>17.1 cells; inhibition of TNF signaling, via use of non-selective TNF inhibitors, exacerbated MS<sup>62,63</sup> and induced new cases of demyelinating disease and neuropathies in patients treated for other inflammatory diseases<sup>64,65</sup>. These effects were likely due to full abrogation of TNF signaling whereas SR3335 selectively inhibited TNF $\alpha$  in T<sub>H</sub>17 and T<sub>H</sub>17.1 cells, leaving T<sub>H</sub>1 and T<sub>H</sub>2 cells intact. While the effects on TNF $\alpha$  were modest, as were those on IL-22, they need to be further explored to determine if the effects are a cause for concern with potential MS therapies, or the mechanism can be further exploited with more potent ROR $\alpha$  inverse agonists for IBD.

While our studies have focused on the positive benefits of inhibiting ROR $\alpha$  in T<sub>H</sub>17 cells under chronic inflammatory conditions, tissue-resident “homeostatic” T<sub>H</sub>17 cells play key, non-pathogenic roles in protection of the mucosal barrier<sup>4</sup>. Furthermore, evidence suggests these homeostatic T<sub>H</sub>17 cells may contribute to the development of chronic inflammatory diseases<sup>4</sup>. Therefore, it is possible that T-cell-specific deletion of ROR $\alpha$ , and/or inhibition of ROR $\alpha$  activity may render the host more susceptible to dissemination of enteric bacteria or infection by pathogenic bacteria, including *Citrobacter rodentium*. However, studies demonstrating transient inhibition or deletion of ROR $\gamma$  activity suggest the host would only be mildly susceptible to *C. rodentium* infection as ILC3s remained intact in mouse hosts<sup>66</sup>. Conversely, a recent report suggests that ROR $\alpha$  is required for the maintenance of ILC2s and ILC3s<sup>67</sup>. Given that conditional T-cell deletion of ROR $\alpha$  would render ILCs intact and use of a ROR $\alpha$  small molecule inhibitor would not completely ablate ROR $\alpha$  activity *in vivo*, it is possible that ROR $\alpha$  function would still be sufficient in ILC3s to control *C. rodentium* infection. However,

this would have to be tested. Thus, we believe that in the absence of, or inhibition of ROR $\alpha$  in T<sub>H</sub>17 cells, the host would be mildly susceptible to bacterial infection at mucosal barriers. Furthermore, a recent report demonstrated that the induction of inflammatory T<sub>H</sub>17 cell responses in the periphery are not influenced by “homeostatic” T<sub>H</sub>17 cells<sup>68</sup>. This data suggests that any ROR $\alpha$ -mediated effects on homeostatic T<sub>H</sub>17 cells would likely have no effect on susceptibility to chronic inflammatory conditions, including EAE. One caveat to these experiments, however, were that they were focused on inflammatory cells generated by *C. rodentium*, not EAE. Therefore, EAE experiments will need to be performed to definitively prove this point.

In summary, we have demonstrated a pathogenic role for ROR $\alpha$  in T<sub>H</sub>17 cell development and chronic inflammation. Our work indicates that targeting this receptor for the treatment of T<sub>H</sub>17-mediated autoimmunity may be an alternative strategy that warrants further investigation.

## Methods

**Mice.** *C57BL/6*, *SJL/J*, *B6.129S7-Rag1<sup>tm1Mom</sup>/J*, stock # 003145 (*Rag1*<sup>−/−</sup>), *B6(Cg)-Rorc<sup>tm3Lit</sup>/J*, stock # 008771 (*Rorc*<sup>fl/fl</sup>), and *Tg(Cd4-Cre)1Cwi/Bflu*, stock # 017336 (*CD4-Cre*) mice, and *B6.SJL-Ptprca<sup>b</sup>Pepe<sup>b</sup>/Boy*, stock # 002014 (*CD45.1*) were purchased from the Jackson Laboratory. The *Rora*<sup>fl/fl</sup> mice were generated on a *C57BL/6* background using a previously published targeting strategy: loxp sites were inserted flanking exon 3 of the *Rora* gene, which causes a premature stop codon early in exon 4<sup>69,70</sup>. *Rora*<sup>fl/fl</sup> × *CD4-Cre* and *Rorc*<sup>fl/fl</sup> × *CD4-Cre* mice were generated by cross breeding *Rora*<sup>fl/fl</sup> or *Rorc*<sup>fl/fl</sup> with *CD4-Cre* mice to produce littermates homozygous for loxp allele and hemizygous for *Cre*. All groups of experimental mice were matched for age and sex and randomly allocated to treatments within cage groups to eliminate litter effects. All experiments were conducted at controlled temperature (22–23 °C), humidity ~60%, and 12 h:12 h light:dark cycles. Mice had access to regular chow (Harlan 2920X) and water, *ad libitum*. For all *in vitro* experiments, mice were killed between 8 and 10 a.m. For all *in vivo* experiments, mice were killed between 7 and 11 a.m. For EAE experiments, mice were immunized between 11 a.m. and 1 p.m. All mice were maintained under specific pathogen free conditions and the Scripps Florida Institutional Animal Care and Use Committee (IACUC) approved all experiments.

**Human samples.** Human blood samples were conducted in accordance with IRB protocols approved by the Institutional Review Board at the Scripps Research Institute (TSRI), OneBlood (Orlando, Florida), and the University of Miami. Blood was obtained following informed written consent from healthy adults or patients with ulcerative colitis. Consenting patients provided clinical history and demographic data at the time of phlebotomy. Institutional review boards at OneBlood and the University of Miami approved all procedures. All forms and documentation that were used obtaining informed consent is stored at OneBlood or the University of Miami. PMBCs were isolated following ficoll density centrifugation and frozen in liquid nitrogen until further analysis. Cryopreserved PBMCs were stored in de-identified and barcoded vials.

**Chemical synthesis and reagents.** SR3335<sup>36</sup> and SR2211<sup>40</sup> have previously been described. T0901317 was purchased from Cayman Chemical (Cat. #71810) and Rifampicin was purchased from Chem-Impex International, Inc. (Cat. # 00260).

**Mouse *in vitro* CD4<sup>+</sup> T cell differentiation.** Naive CD4<sup>+</sup> T cells from spleen and lymph nodes of male and female 8–10-week-old mice were purified after removing the red blood cells using Lympholyte-M solution (Cedarlane Laboratories). Cells were enriched for naive CD4<sup>+</sup> T cells using the mouse naive CD4<sup>+</sup> T Cell Isolation Kit (STEMCELL Technologies, Canada) according to the manufacturer's instruction. If sorting was performed (FACS Aria II; BD Bioscience), the CD4<sup>+</sup>CD25<sup>−</sup>CD62L<sup>hi</sup>CD44<sup>lo</sup> fraction was collected. The conditions for the different T<sub>H</sub> cell subsets were: For T<sub>H</sub>0 (neutral conditions): 5  $\mu$ g/ml anti-IL-4 (clone 11B11, BioLegend) and 5  $\mu$ g/ml anti-IFN $\gamma$  (clone XMG1.2, BioLegend); For T<sub>H</sub>1 conditions: 5  $\mu$ g/ml anti-IL-4, 20 ng/ml IL-12 (R&D Systems), and 10 ng/ml IFN $\gamma$  (R&D Systems); For T<sub>H</sub>2 conditions: 5  $\mu$ g/ml anti-IFN $\gamma$  and 10 ng/ml IL-4 (R&D systems); For T<sub>H</sub>17 conditions: 5  $\mu$ g/ml anti-IFN $\gamma$ , 5  $\mu$ g/ml anti-IL-4 (R&D Systems), and 1.5 ng/ml TGF $\beta$  (R&D Systems) and 30 ng/ml IL-6 (R&D Systems); For iT<sub>H</sub>reg conditions: 5  $\mu$ g/ml anti-IFN $\gamma$ , 5  $\mu$ g/ml anti-IL-4, and 5 ng/ml TGF $\beta$  (R&D Systems); For Tr1 conditions: 20 ng/ml IL-27 (R & D Systems). Other cytokines used for various T<sub>H</sub>17 conditions: IL-1 $\beta$  (10 ng/ml, R&D Systems) and IL-23 (20 ng/ml, R&D Systems).  $1 \times 10^6$  cells/ml of naive CD4<sup>+</sup> T cells were activated with anti-CD3 (clone 2C11, 0.5  $\mu$ g/ml) and anti-CD28 (clone 37.51; 1  $\mu$ g/ml) by precoating plates with 50  $\mu$ g/ml goat anti-hamster IgG. After 48 h, cells were removed from the TCR signal and recultured at a concentration of  $1 \times 10^6$  cells/ml. Four days after activation, all cells were restimulated with 50 ng/ml phorbol-12-myristate-13-acetate

(PMA) (Sigma) and 1 µg/ml ionomycin (Sigma) for 2 h with the addition of GolgiStop (BD Bioscience) for an additional 2 h before intracellular staining. Cells were cultured in IMDM medium (Invitrogen) with 10% FBS, 100 IU/ml penicillin, 100 µg/ml streptomycin, 50 µM β-mercaptoethanol, and 2 mM L-glutamine. All cultures were performed in a volume of 200 µl in 96-well U-bottomed plates. For memory T cell cultures, sorted cells (CCR6<sup>+</sup> or CCR6<sup>-</sup>) were added to 96-well round bottom tissue culture plates (3 × 10<sup>4</sup> cells/well) along with anti-CD3/anti-CD28 coated beads (Invitrogen) and recombinant IL-2 (10U/ml; NCI, Biological Resources Branch) for 6 days and treated as described in the text. On day 6, cells were treated as described above for intracellular cytokine staining.

**Isolation of human PBMCs and T cells.** Human blood samples were collected from OneBlood (Orlando, FL) and processed in accordance with protocols approved by Institutional Review Boards at Scripps Florida. Peripheral blood mononuclear cells (PBMCs) were isolated from healthy donor buffy coats by Ficoll-Paque (Sigma) density gradient centrifugation. Naïve CD4<sup>+</sup> T cells or effector memory CD4<sup>+</sup> T cells were separated using the EasySep Human Naïve CD4<sup>+</sup> T cell isolation kit II or EasySep Human Memory CD4<sup>+</sup> T cell Enrichment Kit, respectively (STEMCELL Technologies, Canada) according to the manufacturer's instructions. Cell purity of >95% was obtained in the majority of donors for the experiments. For UC/healthy donor samples, frozen PBMCs were thawed and incubated overnight in fresh media. Cell viability was assessed the following day following by isolation of naïve CD4<sup>+</sup> T cells following methods outlined above.

**Human in vitro CD4<sup>+</sup> T cell differentiation.** Human T<sub>H</sub>17 cell differentiations were performed as follows: naïve CD4<sup>+</sup> T cells were isolated from buffy coats and cultured in 96-well plates at a density of 2 × 10<sup>5</sup> per well. Cells were activated with 5 µg/ml plate-bound human anti-CD3 (clone OKT3; Bio X Cell) in complete RPMI<sup>43</sup>. For T<sub>H</sub>17 differentiation, recombinant human IL-23 (50 ng/ml) and IL-1β (50 ng/ml) were added at the start of culture. Sorted effector memory T cell populations were cultured as follows: cells were cultured in DMEM supplemented with 10% FBS, 100 IU/ml penicillin, 100 µg/ml streptomycin, 50 µM β-mercaptoethanol, and 2 mM L-glutamine 10 mM HEPES, 1% non-essential amino acids, and 1% Na pyruvate. Purified T cells were activated with anti-CD3 and anti-CD28-coated beads (Dynabeads; Invitrogen) for 3 days. After 48 h, IL-2 (30 U/ml) was added to the culture. On day 3, anti-CD3/anti-CD28 coated beads were removed using Dynabeads magnets (Invitrogen), and cells were maintained with IL-2 for an additional 3 days<sup>47</sup>. DMSO or SR3335 was added at the start of the cultures.

**Flow cytometry.** Surface staining: single cell suspensions prepared from spleen, lymph nodes, CNS, etc. were washed and stained with fluorescence-conjugated antibodies for 20 minutes, washed, then resuspended in FACS buffer (0.5% BSA, 2 mM EDTA in PBS). Intracellular cytokine staining: cells were restimulated with 50 ng/ml PMA and 1 µg/ml ionomycin for 2 h with the addition of GolgiStop (BD Bioscience) for an additional 2 h. Cells were then surface stained using procedures outlined above, fixed and permeabilized using the Foxp3 staining kit (eBioscience). Flow cytometric analysis was performed on a BD LSRII (BD Biosciences) instrument and analyzed using FlowJo software (TreeStar). All antibodies used in experiments are described in Supplementary Table 1.

**FACS sorting of human and mouse effector memory T cells.** All FACS sorting was performed using a FACS Fusion (BD). For sorting of human memory T cell subsets from healthy adult PBMCs, enriched memory CD4<sup>+</sup> T cells (STEMCELL Tech) were stained using the following antibodies: anti-CD4 (BV605); anti-CD25 (PE-CF594); anti-CD45RO (Alexa700); anti-CCR6 (APC); anti-CCR4 (PE-Cy7); anti-CXCR3 (PerCP-Cy5.5); anti-CRTH2, anti-CCR10 (PE; dump); viability (BV510). Stained cells were resuspended in FACS buffer, filtered through a 40-µm filter, and sorted. Sorting of mouse CCR6<sup>+</sup> cells was performed as follows: T cells were isolated from the spleens and lymph nodes and enriched using CD4<sup>+</sup> negative isolation kits from STEMCELL Technologies according to the manufacturer's instructions. Memory (CD25<sup>-</sup>CD62L<sup>lo</sup>CD44<sup>hi</sup>) were further sorted for CCR6 expression by FACS (FACSARIA II)<sup>71</sup>. For more information on antibodies, please see Supplementary Table 1.

**Retroviral transduction.** To generate the RORα retroviral vector, RORα was inserted into a modified MIGR1 vector (Addgene) with additional multiple cloning sites inserted, using the BamHI site and EcoRI site. MIGR1 empty vector was used as a control. MIGR1 RORyT retroviral construct was a gift from Dan Littman (Addgene Plasmid #24069). Virus production: Plat-E cells (Cell Biolabs, Inc.) were cultured in DMEM containing 10% fetal bovine serum, 2mM L-glutamine, and 1% penicillin/streptomycin at 37 °C under standard culture conditions. Plat-E cells were seeded at 350,000 cells/ml in a 6-well plate the day before transfection. In all, 3 µg total retroviral plasmid DNA (1.5 µg MIGR1 plus 1.5 µg pCL-Eco) was transfected using Fugene6 reagent (Promega) according to manufacturer's protocol. Viral supernatant was harvested 48 h post-transfection and used immediately for transduction. For retroviral transduction, naïve CD4<sup>+</sup> T cells were stimulated as indicated with anti-CD3 and anti-CD28 and cultured under T<sub>H</sub>17 conditions. At 24 h post TCR priming, the culture medium was replaced with virus supplemented with 8 µg/ml polybrene. Plates were centrifuged at 1800 rpm for 75 min at 37 °C

and then incubated at 37 °C for 3–4 h. After this time, the medium was replaced with the original media removed before addition of virus.

**Induction and clinical evaluation of EAE.** Chronic (MOG) EAE was induced in 10-week-old, female *Rora*<sup>fl/fl</sup> or *Rora*<sup>fl/fl</sup> × *Cd4-Cre* mice, or WT mice (drug treatments) using EAE induction kits (EK-2110; Hooke Laboratories, Lawrence, MA, USA) according to manufacturer's instructions. Briefly, mice were injected subcutaneously over two sites in the flank with 200 µg/mouse of mouse MOG<sub>35–55</sub> peptide in an emulsion of Complete Freund's Adjuvant (CFA), containing killed *M. tuberculosis*, strain H37Ra. Concentration of killed *M. tuberculosis* was adjusted by lot depending on EAE induction and ranged from ~2–5 mg/mL emulsion. Pertussis toxin was dissolved in PBS and injected i.p. at a range of 200–400 ng/mouse 4 h post-immunization (day 0) and 24 h later. The concentration of pertussis toxin used varied by lot and was determined by dose response studies. For relapsing-remitting EAE (R-EAE), 10-week-old, female SJL/J mice were immunized using EAE induction kits (EK-2120; Hooke Laboratories, Lawrence, MA, USA) according to manufacturer's instructions. Similar induction protocols were used for R-EAE with the exception that 100 µg/mouse of mouse PLP<sub>139–151</sub> peptide in an emulsion of Complete Freund's Adjuvant (CFA), containing 1 mg/mL of killed *M. tuberculosis*, strain H37Ra, was used. Furthermore, 1 injection of 400 ng/mouse of pertussis toxin following immunization (day 0) occurred. As described above, all concentrations were adjusted by lot for consistent EAE induction. Clinical scoring started 7 days post-immunization after which mice were scored daily according to the following criteria: 0, no clinical disease; 1, limp/flaccid tail; 2, limp tail and hind leg weakness; 3, limp tail and complete paralysis of hind limbs; 4, limp tail, complete hind limb and partial front limb paralysis; and 5, quadriplegia or pre-moribund state. Gradations of 0.5 were used when mice exhibited signs that fell between two scores. All scoring was blinded to genotype or treatment and previous scores for each mouse. For drug treatment experiments, SR3335 was dissolved in a 10% DMSO, 10% Tween 80, and 80% H<sub>2</sub>O solution equaling 3 mg/mL and administered intraperitoneally (i.p.) at 30 mg/kg as was vehicle control (10% DMSO, 10% Tween 80, and 80% H<sub>2</sub>O) twice per day (b.i.d). For chronic MOG-induced EAE, the treatment was started the evening of the immunization and continued for the duration of the experiment. Disease was monitored for 28 days or as indicated in the figure legend. For R-EAE, the treatment was started the after the animals recovered from the first wave of disease and continued for the duration of the experiment. For all b.i.d. dosing, animals were dosed at 7 a.m. and 7 p.m. (lights on/lights off). At the end of the experiment, mice were anaesthetized and transcardially perfused with PBS, and spleen, peripheral lymph nodes together with spinal cords were removed for single cell isolation for FACS analysis.

**T-cell transfer model of colitis.** Spleens were collected from 8–10-week-old, female *Rora*<sup>fl/fl</sup> or *Rora*<sup>fl/fl</sup> × *Cd4-Cre* mice to sort naïve CD4<sup>+</sup> T cells. In all, 5 × 10<sup>5</sup> CD4<sup>+</sup>CD25<sup>-</sup>CD62L<sup>hi</sup>CD44<sup>lo</sup> cells suspended in PBS were adoptively transferred i.p. (100 µl/mouse) into 8-week-old, female *Rag1*<sup>-/-</sup> recipient mice<sup>72</sup>. For congenic transfers, similar protocols were used with the exception that naïve female CD45.1 CD4<sup>+</sup> T cells were sorted in lieu of *Rora*<sup>fl/fl</sup> T cells. Post sort, cells were counted, adjusted for cell number, mixed at a 50/50 ratio, and analyzed by flow cytometry to determine equal frequency of the two experimental groups. Once verified, the mixture was injected into female *Rag1*<sup>-/-</sup> recipients. Mice were monitored bi-weekly for body weight change. Beddings were transferred between cages to minimize the impact of microflora on disease development. Mice were killed to assess histological inflammation due to ethical requirements if they reached 80% or less of their original body weight. For the therapeutic evaluation of SR3335 in the T-cell transfer model of colitis, spleens were collected from 8–10-week-old female C57BL/6 mice to sort naïve CD4<sup>+</sup> T cells as described above. In total, 5 × 10<sup>5</sup> sorted naïve CD4<sup>+</sup> T cells were adoptively transferred i.p. (100 µl/mouse) into female *Rag1*<sup>-/-</sup> recipient mice as described above. Three weeks post-transfer, SR3335 was dissolved in a 10% DMSO, 10% Tween 80, and 80% H<sub>2</sub>O solution at 3 mg/mL and administered i.p. at 30 mg/kg as was vehicle control (10% DMSO, 10% Tween 80, and 80% H<sub>2</sub>O) twice per day (b.i.d). Mice were treated for 2 weeks. After the two-week period, mice were killed to collect spleens, mesenteric lymph nodes, and intestines for FACS analysis.

**Mouse intestine tissue end-point collection.** At the termination of the 12-week experiments, the whole colon and ileum (distal 1/3 part of the small intestine) were removed from the mouse. Each segment of the intestine was opened longitudinally, and the fecal contents were gently removed. Colon length and weight were measured and then the colon was dissected in equal halves, designated as 'proximal' and 'distal' colon and snap frozen in dry ice for protein and RNA analysis.

**Histological assessment of intestinal inflammation.** Following overnight fixation in 10% buffered formalin, proximal and distal colon samples were paraffin-embedded, cut in 5 mm sections, and stained with hematoxylin and eosin (H&E). Inflammation was scored in a blinded fashion using a modified scoring system described in Wang et al.<sup>72</sup>. Briefly, each sample was graded on a scale of 0–3 to assess the following four criteria: assessments of markers of severe inflammation (crypt abscesses, ulcers), tissue damage, degree of epithelial hyperplasia and goblet

cell depletion, and inflammatory cell infiltration. Scores for each criteria were added to give an overall inflammation score of 0–12.

**Lamina propria mononuclear cell Isolation from mouse intestine.** At the termination of the 4–6-week experiments, to collect mononuclear cells from the lamina propria of intestine, mouse ileum or colon were dissected, opened longitudinally, rinsed three times in cold PBS, and then DMEM phenol-free medium with 200 U/mL penicillin and 200 mg/mL streptomycin one time to remove the fecal content. Washed intestines were incubated in DMEM with 1 mM DTT at room temperature (RT) on a rocker for 30 min then in DMEM with 0.5 M EDTA for 30 min at RT to remove the mucus layer. After washing twice in DMEM, intestines were then digested in DMEM with Liberase and DNase I at 37 °C in a shaking water bath for 30 min. The cells were then dislodged from the lamina propria and submucosa by vigorous shaking for 30 s. The supernatant containing leukocytes was pooled together by centrifugation at 500 g for 5 min. Cells were further cleaned up by 30%/70% Percoll (Sigma) gradient separation before further study.

**Analysis of thymocytes.** For the measurement of double positive (DP) thymocyte survival kinetics, 7–9-week-old male C57BL/6 mice were treated with compound or vehicle control for 3 days. All compounds were formulated in 15% cremophor at the following concentrations: SR2211 – 2 mg/mL; SR3335 – 3 mg/mL; and administered i.p., b.i.d. Thymii were collected at the termination of the experiment, minced and passed through 70 µm mesh cell strainers. Cell counts were performed prior to cell staining for flow cytometry analysis.

**Quantitative reverse-transcription polymerase chain reaction.** Tissue samples (snap frozen and homogenized) were extracted into TRIzol before RNA purification using RNeasy columns (Zymo Research, CA), followed by cDNA synthesis using iScript (BioRad, CA) containing oligo (dT) and random hexamer primers. qPCR SYBR Green (Roche) was used for quantitative polymerase chain reaction using a HT7900 machine (Life Technologies, CA); passive reference dye ROX was used. Primer efficiencies were determined using complementary DNA and primer dilutions for each gene of interest. Primers used to determine gene expressions can be found in Supplementary Table 2. All gene expression data were normalized to the housekeeping gene  $\beta$ -actin or 18 s.

**Nanostring.** Gene expression was quantified using a custom nCounter probe set containing 55 probe pairs with additional probes for positive and negative controls as well as housekeeping genes. (Nanostring Technologies). Briefly, 30,000 T cells were lysed in 5 µl of freshly made buffer RLT (Qiagen) containing  $\beta$ -ME. Biotin-conjugated capture probes and fluorescent-barcoded reporter probes were hybridized to cell lysates overnight at 65 °C in a thermocycler. The following day, post-hybridization processing occurred on all lysates which were then run on an nCounter SPRINT (Nanostring Technologies) according to the manufacturer's instructions. Raw data were normalized and analyzed using nSolver software (Nanostring Technologies).

**RNA—sequencing and data analysis.** mRNA was extracted from T<sub>H</sub>17 cells on Day 2 (WT vs. ROR $\alpha$  KO cells) or Day 3 (MIGR1 transduced cells) of in vitro differentiation. Total RNA was extracted using Qiagen RNeasy kits, quantified using the Qubit 2.0 Fluorometer (Invitrogen, Carlsbad, CA), and run on the Agilent 2100 Bioanalyzer (Agilent Technologies, Santa Clara, CA) for quality assessment. DNase-treated total RNA (300 ng) was depleted of ribosomal RNA (rRNA) using appropriate probes provided by Illumina (TruSeq Total RNA-seq kit) and further assessed on the bioanalyzer to confirm 18S and 28S rRNA peaks are depleted. rRNA-depleted RNA is processed using the TruSeq Stranded Total RNA sample prep kit (Illumina, San Diego, CA). Briefly, RNA samples are chemically fragmented in a buffer containing divalent cations and heating at 94 °C for 8 min. The fragmented RNA is random hexamer primed and reverse transcribed to generate first strand cDNA. The second strand is synthesized after removing the RNA template and incorporating dUTP in place of dTTP. cDNA is then end repaired and adenylated at their 3' ends. A corresponding 'T' nucleotide on the adapters is utilized for ligating the adapter sequences to the cDNA. The adapter-ligated DNA is purified using magnetic Ampure XP beads and PCR amplified using 12–13 cycles to generate the final libraries. The final libraries are size selected and purified using 1.0 × Ampure XP beads to remove any primer dimers. The final library size is typically 200–600 bp with insert sizes ranging from 80 to 450 bp. Final libraries are validated using bioanalyzer DNA chips and qPCR quantified using primers recognizing the Illumina adapters. Libraries are pooled at equimolar ratios, quantified using qPCR (quantification of only the adapter-ligated libraries) and loaded onto the NextSeq 500 flow cell at 1.8 pM final concentration for pair end 75 bp reads. In total, 20–25 million mappable reads per sample were collected. Demultiplexed and quality filtered raw reads (fastq) generated from the NextSeq 500 were trimmed (adapter sequences) using Flexbar 2.4 and aligned to the reference genome using TopHat version 2.0.9<sup>73</sup>. HT seq-count version 0.6.1 was used to generate gene counts and differential gene expression analysis was performed using Deseq2<sup>74</sup>. The normalized gene counts were used to plot the heatmaps using the heatmap function in Prism. To determine enriched

functional groups in the RNA-seq data, KEGG pathway analysis was performed using DAVID<sup>75,76</sup>.

**Western blot analysis.** T cells were harvested and washed once with phosphate-buffered saline and then incubated for 10 min at 4 °C in 50 µl of TNT lysis buffer (50 mM Tris-Cl, pH 7.5, 150 mM NaCl and 1% Triton X-100) and a complete protease inhibitor mixture (Roche Applied Science). Lysates were then vortexed for 30 s, and then centrifuged at 4 °C for 10 min to clear up. Protein levels in the supernatants were determined using a Coomassie protein assay, ~10 µg of protein from each sample was separated by 10% Tris-glycine gel and then transferred to a polyvinylidene difluoride membrane (Millipore) and immunoblotted with primary antibodies: mouse ROR $\alpha$  (CX-16, Santa Cruz, 1:200 dilution), mouse ROR $\gamma$  (Life Technologies, 1:200 dilution), or  $\beta$ -Actin (Cell Signaling Technology, 1:1000 dilution) and horseradish peroxidase-conjugated (HRP) secondary antibodies (Jackson ImmunoResearch; Polyclonal Donkey Anti Goat IgG, Cat # 705-035-147, Lot # 128117; Polyclonal Donkey Anti-Rat IgG, Cat # 712-135-150, Lot #109032; Polyclonal Goat Anti-Mouse IgG, Cat # 115-035-174, Lot # 143785). All HRP secondary antibodies were used at a 1:10,000 dilution. Detection of the bound antibody by enhanced chemiluminescence was performed according to the manufacturer's instructions (Santa Cruz).

**Cell culture.** HEK293 (American Type Culture Collection) and Plat-E cells (Cell Biolabs, Inc.) were cultured in DMEM (Invitrogen) supplemented with 10% FBS, 2 mM L-glutamine, and 1% penicillin/streptomycin at 37 °C, 5% CO<sub>2</sub> under standard culture conditions. Mouse lymphocytes were cultured in IMDM medium (Invitrogen) with 10% FBS, 100 IU/mL penicillin, 100 µg/ml streptomycin, 50 µM  $\beta$ -mercaptoethanol, and 2 mM L-glutamine. Human lymphocytes were cultured in RPMI medium (Invitrogen) with 10% FBS, 100 IU/mL penicillin, 100 µg/ml streptomycin, 50 µM  $\beta$ -mercaptoethanol, and 2 mM L-glutamine HEPES, and Na pyruvate.

**Luciferase reporter assays.** HEK293 cells were plated 24 h prior to transfection in 96-well plates at a density of 15 × 10<sup>3</sup> cells/well. Transfections were performed using Lipofectamine 3000 (Invitrogen) according to manufacturer's protocol. For drug treatments - 16 h post-transfection, cells were treated with vehicle or compound. Twenty-four hours post-treatment luciferase activity was measured using BriteLite (PerkinElmer Life and Analytical Sciences) and read using an Envision multilabel plate reader (PerkinElmer Life and Analytical Sciences). All values were normalized to DMSO to produce fold induction values.

**Statistical analyses.** Samples sizes, statistical analysis, and *P* values for every experiment are stated in the figures. Raw data from independent experiments can be found in the Source data. Statistical analyses were performed using GraphPad PRISM version 6 and 8 (GraphPad Software, Inc., La Jolla, CA). Student's two-tailed *t*-tests were used for comparison between two groups. To compare differences between groups (i.e. EAE or transfer colitis), unpaired two-tailed nonparametric Mann–Whitney *U* tests with a post hoc test were performed as indicated in the Figure legends. *p* < 0.05 was considered significant.

**Reporting summary.** Further information on research design is available in the Nature Research Reporting Summary linked to this article.

## Data availability

Sequence data have been deposited in the Gene Expression Omnibus (GEO) under accession code [GSE160327](https://www.ncbi.nlm.nih.gov/geo/query/acc.cgi?acc=GSE160327). All other data are in the article and Supplementary Information files or from the corresponding author upon reasonable request. Source data are provided with this paper.

Received: 6 July 2019; Accepted: 23 November 2020;

Published online: 04 January 2021

## References

- Milner, J. D. et al. Impaired T(H)17 cell differentiation in subjects with autosomal dominant hyper-IgE syndrome. *Nature* **452**, 773–776 (2008).
- Puel, A. et al. Chronic mucocutaneous candidiasis in humans with inborn errors of interleukin-17 immunity. *Science* **332**, 65–68 (2011).
- de Beaucoudrey, L. et al. Mutations in STAT3 and IL12RB1 impair the development of human IL-17-producing T cells. *J. Exp. Med.* **205**, 1543–1550 (2008).
- Stockinger, B. & Omenetti, S. The dichotomous nature of T helper 17 cells. *Nat. Rev. Immunol.* **17**, 535–544 (2017).
- Cho, J. H. The genetics and immunopathogenesis of inflammatory bowel disease. *Nat. Rev. Immunol.* **8**, 458–466 (2008).



6. Nair, R. P. et al. Genome-wide scan reveals association of psoriasis with IL-23 and NF-kappaB pathways. *Nat. Genet.* **41**, 199–204 (2009).
7. Ivanov, I. I. et al. The orphan nuclear receptor ROR $\gamma$  directs the differentiation program of proinflammatory IL-17+ T helper cells. *Cell* **126**, 1121–1133 (2006).
8. Yang, X. O. et al. T helper 17 lineage differentiation is programmed by orphan nuclear receptors ROR alpha and ROR gamma. *Immunity* **28**, 29–39 (2008).
9. Lee, Y. et al. Induction and molecular signature of pathogenic TH17 cells. *Nat. Immunol.* **13**, 991–999 (2012).
10. Yang, X. O. et al. Molecular antagonism and plasticity of regulatory and inflammatory T cell programs. *Immunity* **29**, 44–56 (2008).
11. Zhou, L. et al. TGF-beta-induced Foxp3 inhibits T(H)17 cell differentiation by antagonizing ROR $\gamma$  function. *Nature* **453**, 236–240 (2008).
12. Ciofani, M. et al. A validated regulatory network for Th17 cell specification. *Cell* **151**, 289–303 (2012).
13. Hamilton, B. A. et al. Disruption of the nuclear hormone receptor ROR $\alpha$  in staggerer mice. *Nature* **379**, 736–739 (1996).
14. Xiao, S. et al. Small-molecule ROR $\gamma$  antagonists inhibit T helper 17 cell transcriptional network by divergent mechanisms. *Immunity* **40**, 477–489 (2014).
15. Zhang, Y. et al. GENE REGULATION. Discrete functions of nuclear receptor Rev-erbalpha couple metabolism to the clock. *Science* **348**, 1488–1492 (2015).
16. Araujo, L., Khim, P., Mkhikian, H., Mortales, C. L. & Demetriou, M. Glycolysis and glutaminolysis cooperatively control T cell function by limiting metabolite supply to N-glycosylation. *Elife* <https://doi.org/10.7554/eLife.21330> (2017).
17. Berod, L. et al. De novo fatty acid synthesis controls the fate between regulatory T and T helper 17 cells. *Nat. Med.* **20**, 1327–1333 (2014).
18. Gerriets, V. A. et al. Metabolic programming and PDHK1 control CD4+ T cell subsets and inflammation. *J. Clin. Invest.* **125**, 194–207 (2015).
19. Shi, L. Z. et al. HIF1 $\alpha$ -dependent glycolytic pathway orchestrates a metabolic checkpoint for the differentiation of TH17 and Treg cells. *J. Exp. Med.* **208**, 1367–1376 (2011).
20. Xu, T. et al. Metabolic control of TH17 and induced Treg cell balance by an epigenetic mechanism. *Nature* **548**, 228–233 (2017).
21. Shin, B. et al. Mitochondrial oxidative phosphorylation regulates the fate decision between pathogenic Th17 and regulatory T cells. *Cell Rep.* **30**, 1898–1909 e1894 (2020).
22. Wu, L. et al. Niche-selective inhibition of pathogenic Th17 cells by targeting metabolic redundancy. *Cell* **182**, 641–654 e620 (2020).
23. Eftekharian, M. M. et al. RAR-related orphan receptor A (RORA): A new susceptibility gene for multiple sclerosis. *J. Neurol. Sci.* **369**, 259–262 (2016).
24. McGeachy, M. J. & Cua, D. J. The link between IL-23 and Th17 cell-mediated immune pathologies. *Semin. Immunol.* **19**, 372–376 (2007).
25. McGeachy, M. J. et al. TGF-beta and IL-6 drive the production of IL-17 and IL-10 by T cells and restrain T(H)-17 cell-mediated pathology. *Nat. Immunol.* **8**, 1390–1397 (2007).
26. Reboldi, A. et al. C-C chemokine receptor 6-regulated entry of TH-17 cells into the CNS through the choroid plexus is required for the initiation of EAE. *Nat. Immunol.* **10**, 514–523 (2009).
27. Liston, A. et al. Inhibition of CCR6 function reduces the severity of experimental autoimmune encephalomyelitis via effects on the priming phase of the immune response. *J. Immunol.* **182**, 3121–3130 (2009).
28. Morrison, P. J. et al. Th17-cell plasticity in Helicobacter hepaticus-induced intestinal inflammation. *Mucosal Immunol.* **6**, 1143–1156 (2013).
29. Lee, Y. K. et al. Late developmental plasticity in the T helper 17 lineage. *Immunity* **30**, 92–107 (2009).
30. Hirota, K. et al. Fate mapping of IL-17-producing T cells in inflammatory responses. *Nat. Immunol.* **12**, 255–263 (2011).
31. Bending, D. et al. Highly purified Th17 cells from BDC2.5NOD mice convert into Th1-like cells in NOD/SCID recipient mice. *J. Clin. Invest.* **119**, 565–572 (2009).
32. Harbour, S. N., Maynard, C. L., Zindl, C. L., Schoeb, T. R. & Weaver, C. T. Th17 cells give rise to Th1 cells that are required for the pathogenesis of colitis. *Proc. Natl Acad. Sci. USA* **112**, 7061–7066 (2015).
33. Habtezion, A., Nguyen, L. P., Hadeiba, H. & Butcher, E. C. Leukocyte trafficking to the small intestine and colon. *Gastroenterology* **150**, 340–354 (2016).
34. Cosmi, L. et al. Human interleukin 17-producing cells originate from a CD161+CD4+ T cell precursor. *J. Exp. Med.* **205**, 1903–1916 (2008).
35. Annunziato, F. et al. Phenotypic and functional features of human Th17 cells. *J. Exp. Med.* **204**, 1849–1861 (2007).
36. Kumar, N. et al. Identification of SR3335 (ML-176): a synthetic ROR $\alpha$  selective inverse agonist. *ACS Chem. Biol.* **6**, 218–222 (2010).
37. Repa, J. J. et al. Regulation of absorption and ABC1-mediated efflux of cholesterol by RXR heterodimers. *Science* **289**, 1524–1529 (2000).
38. di Masi, A., De Marinis, E., Ascenzi, P. & Marino, M. Nuclear receptors CAR and PXR: Molecular, functional, and biomedical aspects. *Mol. Aspects Med.* **30**, 297–343 (2009).
39. Amir, M. et al. REV-ERB $\alpha$  regulates TH17 cell development and autoimmunity. *Cell Rep.* **25**, 3733–3749.e3738 (2018).
40. Kumar, N. et al. Identification of SR2211: a potent synthetic ROR $\gamma$ -selective modulator. *ACS Chem. Biol.* **7**, 672–677 (2012).
41. El-Behi, M. et al. The encephalitogenicity of T(H)17 cells is dependent on IL-1- and IL-23-induced production of the cytokine GM-CSF. *Nat. Immunol.* **12**, 568–575 (2011).
42. Codarri, L. et al. ROR $\gamma$  drives production of the cytokine GM-CSF in helper T cells, which is essential for the effector phase of autoimmune neuroinflammation. *Nat. Immunol.* **12**, 560–567 (2011).
43. Revu, S. et al. IL-23 and IL-1 $\beta$  drive human Th17 cell differentiation and metabolic reprogramming in absence of CD28 costimulation. *Cell Rep.* **22**, 2642–2653 (2018).
44. Acosta-Rodriguez, E. V. et al. Surface phenotype and antigenic specificity of human interleukin 17-producing T helper memory cells. *Nat. Immunol.* **8**, 639–646 (2007).
45. Sallusto, F., ZIELINSKI, C. E. & LANZAVECCHIA, A. Human Th17 subsets. *Eur. J. Immunol.* **42**, 2215–2220 (2012).
46. Nistala, K. et al. Th17 plasticity in human autoimmune arthritis is driven by the inflammatory environment. *Proc. Natl Acad. Sci. USA* **107**, 14751–14756 (2010).
47. Ramesh, R. et al. Pro-inflammatory human Th17 cells selectively express P-glycoprotein and are refractory to glucocorticoids. *J. Exp. Med.* **211**, 89–104 (2014).
48. Girardi, C. S. et al. Nuclear RXR $\alpha$  and RXR $\beta$  receptors exert distinct and opposite effects on RA<sup>+</sup>-mediated neuroblastoma differentiation. *Biochim. Biophys. Acta Mol. Cell Res.* **1866**, 317–328 (2019).
49. Ramon-Vazquez, A. et al. Common and differential transcriptional actions of nuclear receptors LXRA and LXR $\beta$  in macrophages. *Mol. Cell. Biol.* <https://doi.org/10.1128/MCB.00376-18> (2019).
50. Shimada, K. et al. T-cell-intrinsic receptor interacting protein 2 regulates pathogenic T helper 17 cell differentiation. *Immunity* **49**, 873–885.e877 (2018).
51. Chung, Y. et al. Critical regulation of early Th17 cell differentiation by interleukin-1 signaling. *Immunity* **30**, 576–587 (2009).
52. Ikeda, S. et al. Excess IL-1 signaling enhances the development of Th17 cells by downregulating TGF-beta-induced Foxp3 expression. *J. Immunol.* **192**, 1449–1458 (2014).
53. Malhotra, N. et al. ROR $\alpha$ -expressing T regulatory cells restrain allergic skin inflammation. *Sci. Immunol.* <https://doi.org/10.1126/sciimmunol.aao6923> (2018).
54. Hu, X. et al. Sterol metabolism controls T(H)17 differentiation by generating endogenous ROR $\gamma$  agonists. *Nat. Chem. Biol.* **11**, 141–147 (2015).
55. Santori, F. R. et al. Identification of natural ROR $\gamma$  ligands that regulate the development of lymphoid cells. *Cell Metab.* **21**, 286–298 (2015).
56. Soroosh, P. et al. Oxysterols are agonist ligands of ROR $\gamma$  and drive Th17 cell differentiation. *Proc. Natl Acad. Sci. USA* **111**, 12163–12168 (2014).
57. Rutz, S. et al. Transcription factor c-Maf mediates the TGF-beta-dependent suppression of IL-22 production in T(H)17 cells. *Nat. Immunol.* **12**, 1238–1245 (2011).
58. Neumann, C. et al. c-Maf-dependent Treg cell control of intestinal TH17 cells and IgA establishes host-microbiota homeostasis. *Nat. Immunol.* **20**, 471–481 (2019).
59. Gabrysova, L. et al. c-Maf controls immune responses by regulating disease-specific gene networks and repressing IL-2 in CD4(+) T cells. *Nat. Immunol.* **19**, 497–507 (2018).
60. Xu, M. et al. c-MAF-dependent regulatory T cells mediate immunological tolerance to a gut pathobiont. *Nature* **554**, 373–377 (2018).
61. Brockmann, L., Giannou, A. D., Gagliani, N. & Huber, S. Regulation of TH17 cells and associated cytokines in wound healing, tissue regeneration, and carcinogenesis. *Int. J. Mol. Sci.* <https://doi.org/10.3390/ijms18051033> (2017).
62. van Oosten, B. W. et al. Increased MRI activity and immune activation in two multiple sclerosis patients treated with the monoclonal anti-tumor necrosis factor antibody cA2. *Neurology* **47**, 1531–1534 (1996).
63. TNF neutralization in MS: results of a randomized, placebo-controlled multicenter study. The Lenercept Multiple Sclerosis Study Group and The University of British Columbia MS/MRI Analysis Group. *Neurology* **53**, 457–465 (1999).
64. Sicotte, N. L. & Voskuhl, R. R. Onset of multiple sclerosis associated with anti-TNF therapy. *Neurology* **57**, 1885–1888 (2001).
65. Richez, C., Blanco, P., Laguery, A., Schaefferbeke, T. & Dehais, J. Neuropathy resembling CIDP in patients receiving tumor necrosis factor-alpha blockers. *Neurology* **64**, 1468–1470 (2005).

66. Withers, D. R. et al. Transient inhibition of ROR-gammat therapeutically limits intestinal inflammation by reducing TH17 cells and preserving group 3 innate lymphoid cells. *Nat. Med.* **22**, 319–323 (2016).
67. Lo, B. C. et al. The transcription factor RORalpha preserves ILC3 lineage identity and function during chronic intestinal infection. *J. Immunol.* **203**, 3209–3215 (2019).
68. Omenetti, S. et al. The intestine harbors functionally distinct homeostatic tissue-resident and inflammatory Th17 cells. *Immunity* **51**, 77–89.e76 (2019).
69. Dussault, I., Fawcett, D., Matthyssen, A., Bader, J. A. & Giguere, V. Orphan nuclear receptor ROR alpha-deficient mice display the cerebellar defects of staggerer. *Mech. Dev.* **70**, 147–153 (1998).
70. Billon, C., Sitaula, S. & Burris, T. P. Metabolic characterization of a novel RORalpha knockout mouse model without ataxia. *Front. Endocrinol.* **8**, 141 (2017).
71. Carlson, T. J. et al. Halofuginone-induced amino acid starvation regulates Stat3-dependent Th17 effector function and reduces established autoimmune inflammation. *J. Immunol.* **192**, 2167–2176 (2014).
72. Wang, R. et al. Neutralizing IL-23 is superior to blocking IL-17 in suppressing intestinal inflammation in a spontaneous murine colitis model. *Inflamm. Bowel Dis.* **21**, 973–984 (2015).
73. Trapnell, C., Pachter, L. & Salzberg, S. L. TopHat: discovering splice junctions with RNA-Seq. *Bioinformatics* **25**, 1105–1111 (2009).
74. Anders, S. & Huber, W. Differential expression analysis for sequence count data. *Genome Biol.* **11**, R106 (2010).
75. Huang da, W., Sherman, B. T. & Lempicki, R. A. Systematic and integrative analysis of large gene lists using DAVID bioinformatics resources. *Nat. Protoc.* **4**, 44–57 (2009).
76. Huang da, W., Sherman, B. T. & Lempicki, R. A. Bioinformatics enrichment tools: paths toward the comprehensive functional analysis of large gene lists. *Nucleic Acids Res.* **37**, 1–13 (2009).

## Acknowledgements

We thank the members of the Pipkin lab for their helpful comments of experimental design and analysis as well as the Scripps Florida Genomics and Bioinformatics Cores for library preparation, RNA sequencing, and data analysis. This work was supported by the US National Institutes of Health (1R01AI116885 to L.A.S.). M.A.B. was supported by NSF award 1359369. M.A. was supported through the American Association of Immunologists Careers in Immunology Fellowship Program and the Crohn's and Colitis Foundation of America (#546172).

## Author contributions

L.A.S. conceived the project. T.M.K. synthesized the ligands. L.A.S., R.W., M.A., S.A.M., and S.C., designed/analyzed and/or performed the mouse in vitro assays. L.A.S., M.S.S., A.E., and S.C., designed/analyzed and/or performed the human in vitro assays. L.A.S., R.W., M.A., S.C., and M.A.B., designed, analyzed, and performed the in vivo studies. L.A.S. wrote the manuscript with edits from all authors.

## Competing interests

The authors declare no competing interests.

## Additional information

**Supplementary information** is available for this paper at <https://doi.org/10.1038/s41467-020-20385-9>.

**Correspondence** and requests for materials should be addressed to L.A.S.

**Peer review information** *Nature Communications* thanks Thomas Korn and the other, anonymous reviewer(s) for their contribution to the peer review of this work.

**Reprints and permission information** is available at <http://www.nature.com/reprints>

**Publisher's note** Springer Nature remains neutral with regard to jurisdictional claims in published maps and institutional affiliations.



**Open Access** This article is licensed under a Creative Commons Attribution 4.0 International License, which permits use, sharing, adaptation, distribution and reproduction in any medium or format, as long as you give appropriate credit to the original author(s) and the source, provide a link to the Creative Commons license, and indicate if changes were made. The images or other third party material in this article are included in the article's Creative Commons license, unless indicated otherwise in a credit line to the material. If material is not included in the article's Creative Commons license and your intended use is not permitted by statutory regulation or exceeds the permitted use, you will need to obtain permission directly from the copyright holder. To view a copy of this license, visit <http://creativecommons.org/licenses/by/4.0/>.

© The Author(s) 2021